Thesis for the Degree of Master of Science

Heat Losses in Conventional- and Insulated Exhaust Ports

Jonathan Jones

LUND
UNIVERSITY

Department of Energy Sciences

Division of Combustion Engines

LTH

Lund, Sweden 2015

Abstract

This thesis was carried out at the Division of Combustion Engines within the Faculty of Engineering of Lund University. The thesis was part of a project funded by external parties, with the goal of generating inputs for the creation of insulated exhaust ports. As of today, conventional exhaust ports lose significant heat as they transport hot gas remnants from the cylinder to the exhaust manifold. With insulation, heat and thus potential work can be made available in subsequent steps.

The quantitative inputs were derived from simulative experiments using GT-Power, a widely used software within the automotive industry. The model was adapted to a proposed engine concept which is to be used in later experimental research conducted at Lund University.

The goal of the thesis was to assess a variety of insulating actions and applications to date, but also to give new and practically doable design suggestions with respect to the available timeframe. Since the design of the ports was coupled to the proposed engine setup, care had to be taken to physical constraints induced by that same setup. Another goal was to quantify the relative decrease in heat losses between conventional- and insulated ports, giving justification to insulation procedures.

One insulation setup was deemed applicable and thus implemented in the GT-Power model. This setup consisted of layers with three different materials; cast iron, ceramic insulation and a steel casing. The thickness of each layer was varied in different simulation sweeps, with respect to geometrical constraints. It was found that the best theoretical reduction in heat losses, compared to the conventional ports, was 85.6 %. This was based on a mean flowing diameter of 38 mm inside the ports. However, this result was also based on a non-advised cast iron thickness of 1.5 mm. From a production point of view, this thickness was limited to 3 mm. Using this as a restraint, an 82 % overall reduction in heat losses was observed from the simulations.

Another finding was that the insulation thickness was more significant than the optimization of flow area available to the exhaust gases. Hence, for future development, it is recommended to possibly revise and reduce the original flow area in order to allocate more space to thicker layers of insulating materials.

Acknowledgements

First of all I would like to thank my supervisor, Bengt Johansson, for giving me the opportunity to perform this thesis and for giving me valuable feedback during the course of my work.

I would also like to give a special thanks to my daily supervisor, Nhut Lam, who provided me with a consistent helping hand during my entire stay at the division. Even though Nhut was busy with his own PhD studies, he was never bothered with questions. He always took the required time to provide me with valuable feedback and critic. Big thanks!

Last but not least, I would like to thank professors Per Tunestål and Martin Tunér for examining and approving my report.

Table of Contents

1 Introduction

This thesis work was carried out at the Division of Combustion Engines within the Faculty of Engineering of Lund University. The thesis was part of a project funded by external parties, with the goal of generating inputs for the creation of insulated exhaust ports. These inputs were derived from simulative experiments using GT-Power, a widely used software within the automotive industry.

1.1 Motivation

The lifestyle within the modern society has become highly dependent on different means of transportation, enabling vast movement through a variety of different transportation means. However, the environmental cost of such transportation is beginning to take its toll on a global level because of the associated greenhouse emission. As a consequence, political forces and regulations have been put in place to ensure that future research strive for more efficient fuel consumption.

One example of such measures is the 20-20-20 package in the EU, where key objectives have been set for the year of 2020. The package seeks to reduce the total greenhouse gas emissions by 20 % compared to levels from 1990, increase the share of consumption from renewable sources to 20 % and to reach a 20 % improvement in the EU's energy efficiency. As of today, transportation is responsible for around a quarter of EU's greenhouse gas emission, with one fifth of EU's total CO_2 emissions coming from road transportation [1].

From an automotive engineer's perspective, this boils down to demands for developing more fuel efficient vehicles within road transportation, resulting in less CO_2 emissions per unit volume of fuel. Considering the fact that roughly one-third of the total fuel input energy is converted into useful road work, it is obvious that research must focus on finding improvements along the energy conversion path.

1.2 Thesis workflow

In this thesis, energy conversions will be discussed briefly, along with the basic designs and principles that cause them. However, the main focus will early on shift to losses that are connected to heat dissipation and its distribution between different components within the combustion engines, focusing on the exhaust ports.

Early parts of the thesis will focus on the traditional combustion engine concepts, highlighting the most severe flaws through a step-by-step approach. Following that section, advanced engine concepts will be explained and put into relation with the traditional engine concepts. As will be seen, some flaws are reduced in advanced concepts, while some issues still require improved innovations. The goal with this walkthrough is to pinpoint and highlight flaws along the conversion path and to give justification to a newly proposed engine concept.

The thesis seek to motivate a practical implementation of insulated exhaust ports, designed specifically for an engine concept called the *Double Compression Expansion Engine (DCEE)*. This engine concept is highly dependent on the exhaust ports' abilities to preserve energy as exhaust gases flow through them after combustion. The underlying reason for this will be touched upon in a dedicated section describing the importance of the *DCEE-cycle.* In addition, the same section will give transparency and understanding to the chosen input values that are used in the following simulative experiments.

The simulated experiments will be conducted using an industry acknowledged software called GT-Power. The software itself and its input parameters will be described briefly, linked to the *DCEE-cycle* prerequisites. However, most of the focus will be dedicated to describing the fundamental and underlying physics generating the results. Hence, the main theoretical background of this report is

based on *heat transfer mechanisms*, rather than explaining the software itself. The goal is to provide the reader with enough theory in order to successfully assess and criticize the simulated numbers qualitatively.

Prior to the simulations, a study on different insulating application is performed, reviewing previous work done in reducing heat losses through insulation. The focus is kept to the exhaust ports, but some prior engine insulation experiments are also assessed in order to see if any applications can be adapted and fitted to the exhaust ports using the same kind of philosophies. The different applications are divided into cases, highlighting pros and cons from a production perspective. Hence, the winning case used for simulative purposes is accounting for practical limitations in the insulating process.

1.3 Thesis boundaries

The GT-Power simulations will focus on the reduction of heat losses going from conventional- to insulated exhaust ports. Hence, other parameters such as corresponding emissions and the overall brake efficiency for the whole cycle are not considered. In addition, it is assumed that the chosen case for insulation can be developed and implemented successfully. This assumption is based on professional feedback from manufacturing parties.

The new and insulated exhaust ports will not be tested for endurance issues linked to thermal and mechanical load in the form of e.g. vibrations, degradation or fatiguing operations. In addition, no major modifications are allowed in the exhaust ports at this stage of research due to deadline schedule of the project. Shorter channels, twisting of channels and manipulation of surrounding water channel are all considered major modifications at this stage and hence too time consuming.

Access to technical papers and documentations in the SAE register is limited to publications from 1998 and forward. Any research in the same register from past years was unavailable for the literature study in this thesis.

2 Background

As of today, the road transportation sector is dominated by two different types of internal combustion engines, namely the *Spark-Ignition Engine (SI-engine)* and the *Compression-Ignition Engine (CI-engine).* The engine of choice depends on the required specifications, such as emissions, cost, power ratios and efficiency, just to name a few. The different characteristics are inherited in the design and working principle of the respective engine concept.

2.1 SI- and CI-engines

The *spark-ignition* (SI) engine initiate combustion by producing a spark discharge at the top of the cylinder head. The discharge ignites a premixed charge of fuel and air, starting a chain reaction of heat release in the cylinder. The flame from the ignition eventually propagates through the cylinder volume, continuously releasing heat and producing effective pressure on the piston, yielding a work output through the crankshaft that is mechanically connected to the piston motion.

The *compression-ignition* (CI) engine is similar to the SI-engine from a design point of view, with the same core components such as piston, cylinder and valves. The main difference lies in the mode of operation. In the CI-engine, only air is sucked into the cylinder during the intake stroke. The same air is then compressed in the following compression stroke, resulting in high temperature and pressure. The CI-engine uses a higher compression ratio than the SI-engine, consequently yielding even higher gas temperature and pressure after compression. The fuel itself is added with high pressure (500-2000 bar) at the end of the compression stroke, when the piston is close to the top dead center, i.e. close to the cylinder head [2]. The injection of fuel produce fluid motion and hence a mixing effect between existing air and supplied fuel, resulting in auto-ignition due to the high temperature and pressure, resulting in a continuous heat release and effective pressure on the piston, which exerts a power output through the crankshaft in analogy with the SI-engine.

2.2 Different stroke applications

Independent of the type of traditional engine, a complete cycle can be achieved either with two or four strokes. The difference is defined by how many turns the crankshaft makes in order to complete a full work cycle. One complete turn is done in a two stroke cycle, while two turns are required in the four stroke application.

In the following demonstration of the different strokes, an SI-engine design is used, i.e. an air/fuel ratio of gas enters the intake and combustion is initiated with a spark-plug.

2.2.1 Four-stroke cycle

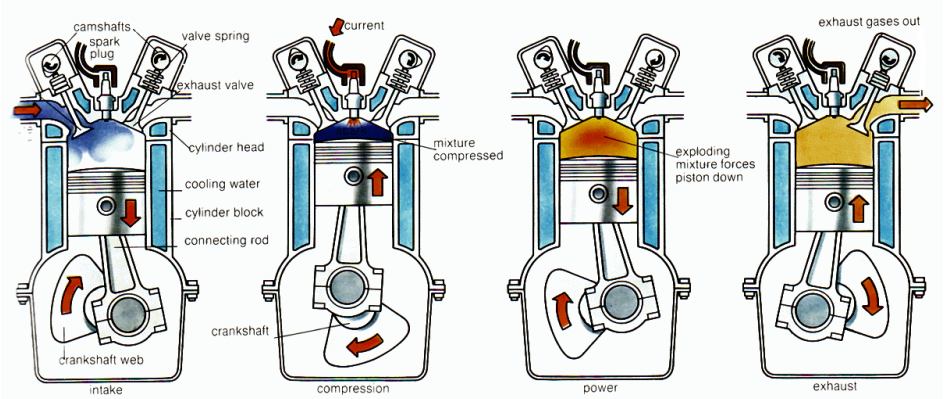

Figure 1 - Four-stroke cycle, SI-engine [3]

According to figure 1, the cycle can be visualized with 4 different steps. During the *intake,* the piston moves towards the bottom center while the open intake valve allows for fuel/air to be sucked into the cylinder, driven by a constant pressure and a continuous volume increase. This stroke is followed by *compression,* during which the valves are closed while the volume decreases thanks to the pistons upward movement. At the end of this stroke, combustion starts as a result of spark-ignition at the top of the cylinder, starting the *power* stroke. The combustion releases energy in the fuel, increasing the pressure. Due to this, the piston moves downwards, yielding a work output on the crankshaft. At the bottom of the cylinder, the exhaust valve opens, initiating the *exhaust* stroke. Due to this, the pressure decreases rapidly and the burnt gases are pushed out to the exhaust during the pistons final movement upwards. At the top center, the exhaust valve closes and the cycle can be repeated once more [2].

2.2.2 Two-stroke cycle

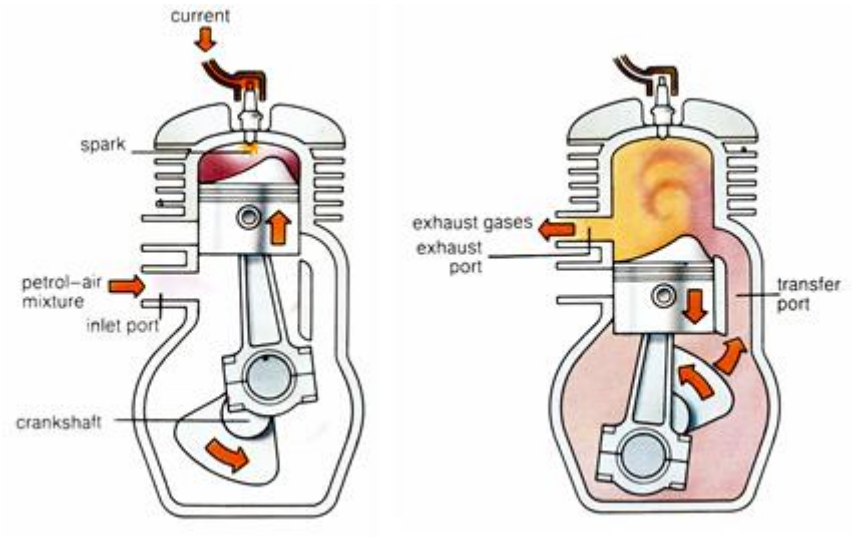

Figure 2 - Two-stroke cycle, SI-engine [4]

According to figure 2, the cycle can be visualized with two different steps. In the two-stroke cycle, compression and fuel/air intake occur simultaneously. The compression starts as soon as the piston completely obstructs the exhaust port. During the upward motion of the piston, the air/fuel mixture is pulled into the cylinder via the inlet port as a result of the increasing volume in the lower section. Once the piston reaches its top center, the gas mixture is ignited with the spark-plug. The combustion releases energy in the fuel, increasing the pressure. Due to this, the piston moves downwards, yielding a work output on the crankshaft.

Eventually, the exhaust ports will be fully open, immediately pushing some of the burnt gases out to the exhaust, lowering the pressure in the cylinder. The continuing blowdown motion uses the recent intake of fresh air/fuel mixture to push the remaining burnt gases through the transfer port and finally out through the exhaust port. This gas exchange will continue until the exhaust port is fully covered once again, by the pistons upward movement. At that point, the cycle can be repeated once more [2].

2.3 Losses in traditional SI- and CI-engines

The *Compression-Ignition* engines (CI) and *Spark-Ignition* engines (SI), hereby referred to as *traditional engine concepts,* are subjected to a variety of losses along the energy conversion path through the engine. The provided fuel and its energy content can be translated into the corresponding pressure *FuelMEP,* recognized as the origin source of energy. From there, different steps and conversions will continuously peel energy and eventually result in a brake mean effective pressure *BMEP,* which will

exert the net pressure on the piston and produce effective work through the crankshaft. This cycle of conversions can be visualized in the energy conversion diagram presented in figure 3 below.

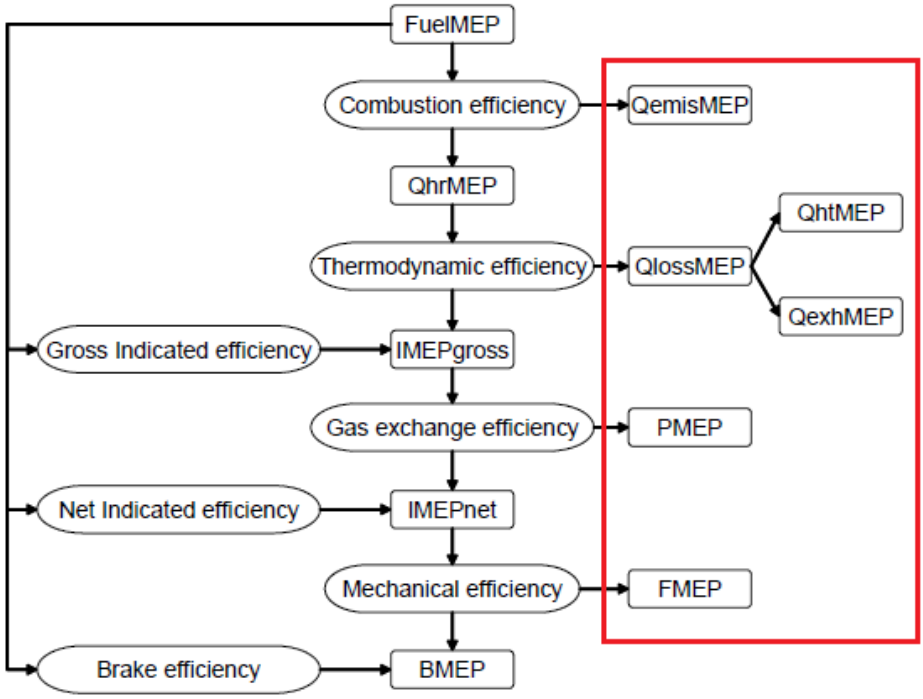

Figure 3 - Energy conversion chart with energy expressed as mean effective pressure (MEP) [5]

The engine's ability to convert chemically stored energy (*FuelMEP)* into useful work through the brake mean effective pressure (*BMEP)* can be expressed as the brake efficiency η_b and is defined as following:

$$\eta_b = \frac{BMEP}{FuelMEP} \tag{1}$$

Each step is coupled to an efficiency, generating a new mean effective pressure downstream while losing some energy equivalent pressure in the process. The total mean effective loss in pressure can be divided into four categories, highlighted within the red box in figure 3.

QemisMEP is accountable for the first loss and hence the first peeling of energy. This loss of pressure occurs as a result of incomplete combustion, linking it to the combustion efficiency. *QlossMEP* describes two different losses related to thermodynamics in the cycle, giving the thermal efficiency. This loss can be split into the categories *QhtMEP,* which covers the heat losses within and through the confinement of the engine, and *QexhMEP,* accounting for pure enthalpy loss from discharging exhaust gases into ambient surroundings. *PMEP* is connected to the gas exchange efficiency, thus dependent on the cylinder's ability to exchange burnt gases with new fresh gases. FMEP is regarded as the final loss in the cycle, accounting for frictional losses and a determination of the mechanical efficiency [2].

As of today, a quantification of the different values of efficiencies can be determined thanks to extensive experimental data. Table 2-1 highlights some of the current reported efficiencies. However, it is important to emphasize that these numbers represent best point values.

Table 2-1: Typical efficiencies obtained in current NA SI- and turbocharged CI-engines [5].

	Naturally Aspirated (NA) SI-engine	Turbocharged CI-engine
Combustion efficiency	95-98%	99.9%
Thermodynamic efficiency	35%	50%
Gas exchange efficiency	98%	104%
Mechanical efficiency	97%	94%
Brake efficiency	32-33%[1]	44%

The thermodynamic efficiency has the lowest quantitative value, making it responsible to a high degree for the rather low brake efficiency. However, the values for CI-engines excel when compared to SI-engines. This is mainly due to the possibility for higher compression ratios in the CI-engines since knock is not an issue. Currently, the highest ever reported thermal efficiency is stated to be at 59 % [6], which is an increase of almost 69 % compared to the standard value of e.g. SI-engines according to table 2-1. However, the thermodynamic efficiency is strongly limited by a constraint induced by the second law of thermodynamics. This limits the maximum theoretical efficiency according to equation 2 [7].

$$\eta = 1 - \frac{T_{cold}}{T_{hot}} \tag{2}$$

An additional aspect related to the thermal efficiency is the fact that it accounts for both *QhtMEP* and *QexhMEP.* Consequently, if heat transfer within the engine is reduced (*QhtMEP),* the enthalpy loss through the exhausts (*QexhMEP)* must not increase by a corresponding amount. If such is the case, a simple reallocation of the energy loss has occurred, resulting in zero net increase in thermodynamic efficiency. As can be seen later one, this has been a problem in recent studies [8].

2.4 Distribution of heat losses

The net heat losses through *QhtMEP* can be divided and traced to different parts of the engine's cylinders. The heat loss distribution is well know from previous studies and by examining figure 4, one can conclude that the cylinder ports constitute a substantial bottleneck from an energy loss perspective. The cylinder valves are second in place, closely followed by the liner, piston and cylinder head, with almost equal distribution. The distribution highlights the potential of using heat reduction measures, especially for the cylinder ports. However, practical application of such measures are not as easy for every part, especially in the case with the liner. Due to friction between the liner and the moving piston, lubrication is an important aspect. Reducing heat losses through the liner will also lead to increased temperatures, which might cause problems such as decomposing of lubrication. The argument of today is therefor to continue using conventional cooling for the liner. This argument is further strengthened by the fact that the heat flux will be at its highest near the TDC (top dead center), where a relatively small cylinder area will participate in the heat transfer. The remaining components listed in figure 4 are all situated at the top of the cylinder, apart from the periodic movement of the piston [8].

[1] The brake efficiency calculated for the SI-engine is the multiple of all the cited part efficiencies. The corresponding brake efficiency for the turbocharged CI-engine is an independently reported value.

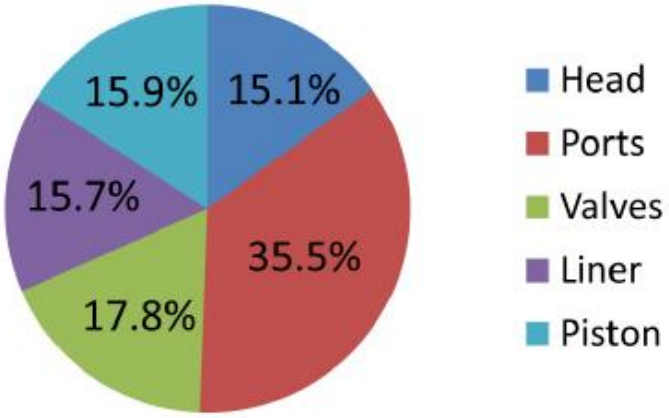

Figure 4 - Heat transfer distribution in a conventionally cooled SI-engine

2.5 Reducing heat losses

Apart from the traditional SI- and CI-engine, modern day concepts have made progress when it comes to increasing the best point of brake efficiency. Different paths depend on different philosophies, which will be briefly discussed in the following sections.

2.5.1 Lowering gas temperature

The following concepts focus on reducing the gas mixture temperature in the cylinder. Through different measures, such as combustion timing and dilution, it is possible to reduce the temperature gradient between gas mixture and cylinder wall, ultimately reducing the in-cylinder heat transfer. The concept focuses on bringing combustion temperatures slightly closer to the cylinder surface temperatures, closing the temperature gap that is highly responsible for heat losses.

2.5.1.1 HCCI

In Homogenous Charge Compression Ignition (HCCI) the air and fuel is mixed before combustion, similar to the mixing process of an SI-engine. The difference is that the ignition itself is not done with a spark plug, instead, the ignition is driven by compression, like in the CI-engine. The HCCI engine is able to achieve higher brake efficiency than traditional engine concepts, and is also very effective in reducing NO_x emissions, thanks to lower peak temperatures. This is mainly due to the fact that the combustion process is very lean, ranging from 2.5-5 in lambda values, with a sweet spot of around lambda = 3. HCCI favors diluted mixtures of fuel and air, being beneficial for reducing heat losses in the cylinder [9]. This is due to the fact that dilution lowers the peak cylinder temperatures, resulting in reduced heat losses [8].

The HCCI manages to reach efficiencies that are in level with the Diesel engine, while keeping emissions of NO_x very low, like in the gasoline engine. The HCCI is also effective in reducing PM (Particulate Matter) emissions. It basically combines two major benefits from the conventional diesel and gasoline engines, respectively. However, the HCCI has problems with power density, and the maximum produced power is around 90 % of what the Diesel engine produces, according to experimental tests at the division of combustion engines in Lund [9]. Another drawback is the problem with controlling the combustion process, i.e. the ignition timing. This is due to the fact that for HCCI the ignition timing is not controlled by a spark as for the SI-engine, neither is it controlled like in a conventional CI combustion, using injection timing for control. That leaves an option of control purely based on chemical kinetics [10].

Recent experiments conducted at Lund University have shown that the thermal efficiency can reach values of around 54 % by utilizing Low Temperature Combustion (LTC), with a reported BMEP of 5 bar. Although this was a significant increase compared to the traditional SI-engine, other parameters were lacking, such as gas exchange efficiency, combustion efficiency and mechanical efficiency. All in all, the resulting brake efficiency was not significantly higher than that of traditional CI-engines [11].

2.5.1.2 PPC

In Partially Premixed Combustion (PPC), the idea is to inject fuel before combustion starts in the cylinder, allowing partial mixing of fuel and air. In order to allow time for this premixing before ignition, parameters such as compression ratio, usage of exhaust gas recirculation (EGR), inlet temperature and fuel properties are varied and assessed. The heat release process in PPC can be more arbitrarily controlled since the sequence of fuel injections is varied in relation to the crank angle, heavily affecting the amount of homogenous charge, i.e. the amount of pre-mixing.

Since the combustion process can be manipulated to a higher degree than in traditional combustion engines, one can study the trade-off relation between having a quick and early heat release, leading to low exhaust losses but high heat losses per sub-volume of the cylinder walls and head, or vice versa, having an extended heat release with lower heat losses to the walls but more heat being dissipated through exhaust gases. This re-allocation is linked to the fact that in the latter case, the heat has less available travel length to insert force onto the piston, leaving more remnant energy at the end of the power stroke, which is later discharged as exhaust. Generally speaking, highly diluted mixtures will yield lower overall heat losses [12].

Recent experiments show that there can be significant gains in thermal efficiency while utilizing PPC, with values of around 57 %. This is a substantial increase compared to both conventional SI- and CI-engines, but also compared to HCCI. The drawback in this case was linked to problems with gas exchange- and mechanical efficiencies due to low loads. These efficiencies were however slightly increased with higher load, while thermal efficiency dropped slightly. All in all, the best achieved brake efficiency was at 48.5 % [13].

2.5.2 Increasing surface temperature

An alternative to reducing the temperature of the gas mixture in the cylinder is to focus on increasing the surface temperature by utilizing isolative materials. This will close the temperature gap to the combustion temperatures, ultimately lowering the heat transfer losses since the temperature gradient between gas and wall will be less aggressive.

2.5.2.1 LHRE

The Low Heat Rejection Engine (LHRE) is a concept idea that has been around for quite a while, with conducted experiments since decades back. The foundation of the concept is heavily based on current issues with heat transfer and exhaust emissions. The approach for reaching this low heat rejection is based on the application of different degrees of insulation within the engine of choice. Components that have been subjected to insulation are e.g. exhaust ports, pistons, cylinder heads, valves and cylinder liners. Regarding the insulation material, ceramic parts and coatings have proven to be effective in insulating the engine.

Many experiments have shown that the LHR engine manages to reduce heat transfer through insulation. However, the increase in overall engine performance, emissions and brake efficiency have been far from significant in relation to the reduced heat transfer [14]. Some research also resulted in increased wall heat transfer when using insulation. This phenomena was traced to something called “convective vive” and it is introduced due to a more reactive boundary layer from the insulation [15]. However, in experiments where heat transfer was reduced, it was shown that a large fraction of the

heat was instead just redirected to the exhausts, having a small or non-existent increase to the overall engine efficiency. This indicates the crucial necessity to make use of the exhaust enthalpy in an efficient matter, otherwise the benefits of using LHRE goes to waste.

Another issue with LHRE is related to the increased working temperature in the cylinder, causing lubricants to decompose at a higher rate than in conventional cooled engines. The higher in-cylinder temperatures have also shown problems with shortening of the ignition delay, resulting in a decrease in the proportion of premixed combustion [8]. There are also issues with pure material properties, especially regarding the choice of insulation. The insulating material must be able to withstand the harsh cylinder conditions by having high strength, high fracture toughness, high thermal resistance and temperature capability. Other parameters such as expansion coefficient and chemical inertness are important for resisting erosion and corrosion. In addition, the material must have low thermal conductivity and low specific heat in order to achieve the desired insulating effect [16].

3 Engine concept of the thesis

Taking inspiration from the previously mentioned traditional and advanced engine concepts, a novel engine concept will be used as basis for the thesis simulations. The idea of the concept is to minimize some of the prescribed losses by splitting the traditional four-stroke cycle into two separate cycles. The splitting results in a rather different setup compared to the ones used in tradition engines, where the gas mixture is compressed and expanded once, all in the same cylinder. Instead, the gas mixture is compressed and expanded twice in two separate cylinders, giving two very different operating conditions in each cylinder. An engine with these core operating procedures is referred to as the *Double Compression Expansion Engine (DCEE)* [5].

The system layout of the DCEE engine can be visualized in figure 5. As can be seen, there are two different cylinders. Each cylinder belong to a different cycle, based on operational pressure. The low pressure cylinder (LP) belongs to the LP-cycle, depicted to the right in figure 5, while the high pressure (HP) cylinder belongs to the HP-cycle, depicted to the left in figure 5.

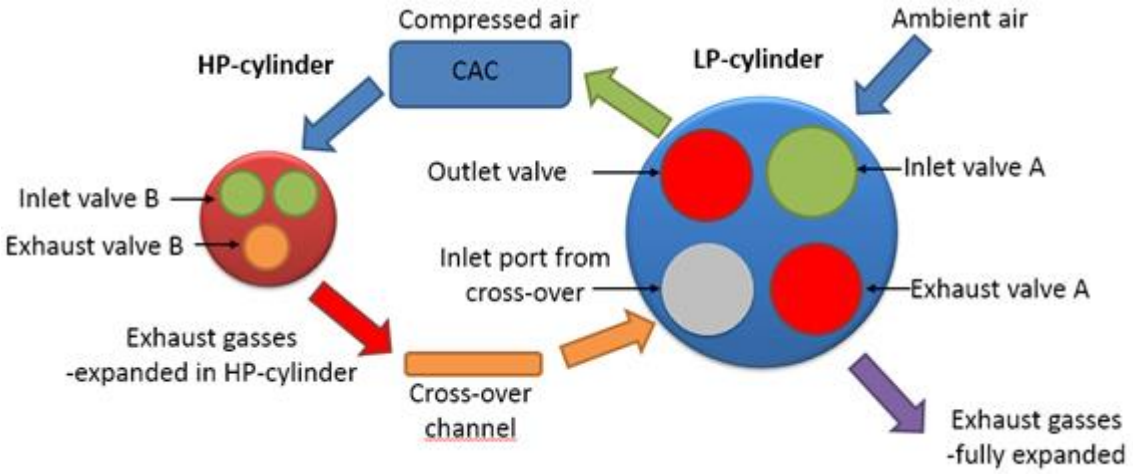

Figure 5 - Working principle of the DCEE engine concept [5]

3.1 Working principle

One of the two purposes of the LP-cylinder is to compress ambient air, entering through the inlet valve A. The resulting boost pressure is then redirected to the HP-Cylinder through the outlet valve. The second purpose is to expand the combusted gas mixture coming from the HP-cylinder. This gas mixture is already partially expanded in the HP-cylinder during the combustion stroke. Consequently, the overall peak cylinder pressure (PCP) in the LP-cylinder, regardless of compression or expansion, will be significantly lower than in a conventional combustion cylinder. This will enable a low friction design of the cylinder, ultimately lowering energy losses due to friction, lowering FMEP. However, this is countered to a smaller extent by increased pumping losses, PMEP, due to the fact that each cylinder only works with one valve open for each intake/exhaust stroke [5]. In a conventional setup, there are usually two valves operating for the corresponding strokes.

The HP-cylinder is designed for very high loads, with BMEPs reaching between 30 and 75 bar. This is possible due to the boosted air transfer from the LP-cycle. However, the PCP is estimated to reach a level of 300 bar. This level of PCP will require a rigid design, capable of handling the peak pressures. The drawback of such a design will be high values of FMEP losses. This is to some extend countered by having a 6 to 12 times smaller displacement than in the case with the LP-cylinder, reducing some friction. Further, the increase in load is more significant than the corresponding increase in FMEP losses, resulting in acceptable levels of mechanical efficiencies.

After the power-stroke in the HP-cylinder, the exhaust gases are to be transported to the LP-cylinder for over-expansion, granting more work output on the crankshaft. This mechanical regeneration allows for increased fuel efficiency. However, the expansion is only as good as the amount of energy that is allowed to pass from the HP- to the LP-cycle [5].

As discussed in the introduction, the efficiency of such transfer will be highly dependent on the amount of heat loss in the cylinder head, specifically in the exhaust ports denoted as “Cross-over channel” in figure 5. This channel is considered a major Achilles heel of the *DCEE* design, and for this reason, focus will lie on reducing losses in these exhaust ports.

4 Methodology and heat transfer theory

This section will entail the fundamental knowledge needed to understand and implement the model used for simulative purposes. The section is divided into three parts; *GT-Power*, *Exhaust ports geometry* and *heat transfer mechanics*. The first section briefly describes the simulation software, with a visualization of the software interface. The second and third part show the applied geometry and the physics behind the heat transfers through the ports, respectively.

4.1 GT-Power

The experimental simulations are realized using the industry approved software GT-Power. The software is commonly applied in conjunction or in advance of assembling a real test rig, enabling quick overviews of engine cycle parameters and results. Hence, the software gives justified hints to parameter tweaking and overall design improvements, lowering the probabilities of designing a faulty rig. However, like any other software, it is not an unbiased reality interpretation. Gt-Power requires qualitative critic that requires knowledge of underlying physics from the user. For this reason, the chapter "*Heat transfer mechanics*" will try to fill any gap of heat transfer knowledge.

In order to secure unbiased results from GT-Power, post-examination is done in order to validate the model and input/output parameters. Figure 6 below shows the interface of the software, with the inlet ports and valves connected to the outlet valves and exhaust ports via the combustor, representing the HP-cylinder. The far left manifold is fed by a similar setup where ambient air is compressed, and the far right manifold represents the inlet before the LP-cylinder.

- Check for convergence in all calculations, no oscillations must be present.
- Quantitative assessment of simulated values, especially by consulting the heat transfer theory in section 4.3.
- Allowing enough iterative power, i.e. allowing for appropriate number of iterations in each simulation step.
- Post processing of simulations to check for warnings like abruptions, interferences or cancelled operations.
- The phenomena of chocking was examined in order to correctly assess the output data from the simulations. It was concluded that chocking does not occur in any of the simulated cases, reducing the complexity of flow characteristics.

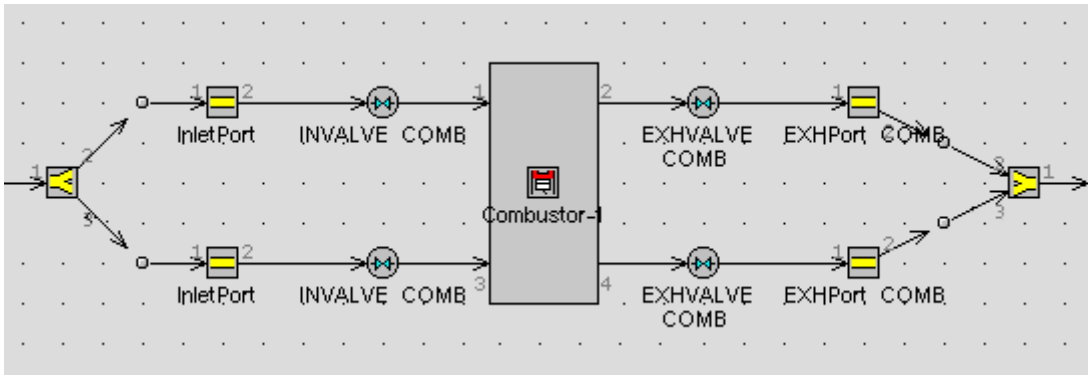

Figure 6 - GT-Power interface, highlighting the HP-cylinder combustor

4.2 Exhaust ports geometry

Due to the isolative materials interference with ignition delay and overall heat release, the focus of this thesis will be concentrated to the heat losses in the exhaust ports, decoupled from the combustion process in the HP-cylinder. Fortunately, the relative heat loss in the exhaust ports, according to figure 4, has a significant impact to the total heat loss within the cylinder of a conventional engine. For this reason, all heat- and isolative analysis from this point onward, will be applicable to the exhaust ports only.

The exhaust ports can be visualized in figure 7 below. The figure shows the exhaust ports in their original state and illustrates the cross-section of two exhaust channels, one from each valve in the cylinder, merging into one common channel. The model belongs to the 13 liter Medium Duty Diesel engine (MD13) that is planned to be utilized in later experiments. The yellow marking highlights the entry to the exhaust ports, where the burnt gas mixture will enter during the exhaust stroke. The two individual channels will merge roughly halfway through the ports, forming one larger cylindrical channel. The mixture is finally discharged to the exhaust manifold, marked in red.

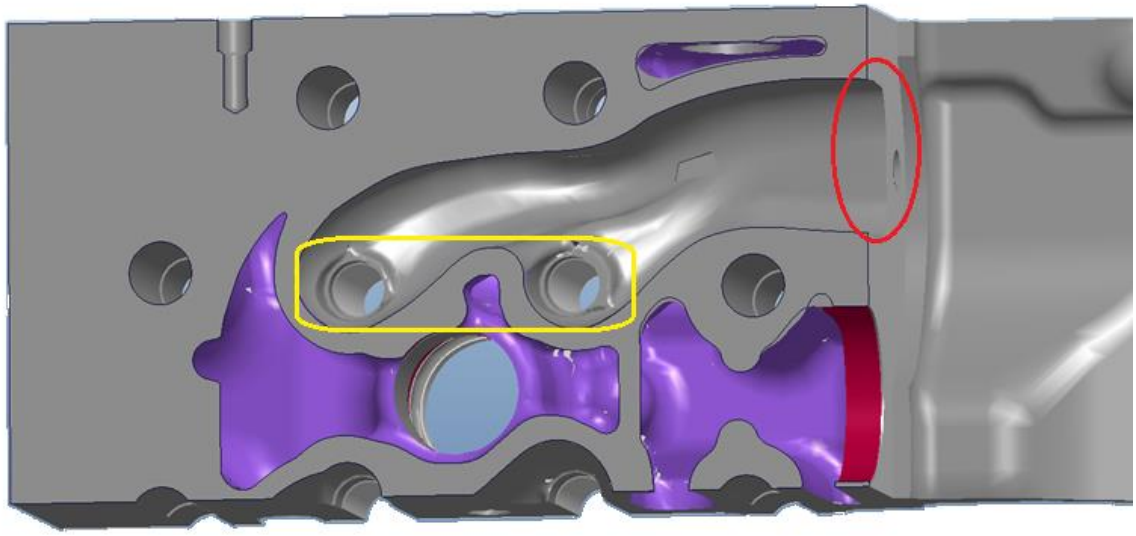

Figure 7 - CAD illustration of dual exhaust ports from a conventional MD13 engine

In order to quantify the heat transfer process in the exhaust ports, a reference model must be adapted and implemented in GT-Power from the original design of such channels. Hence, the exhaust ports are simplified to be treated as two cylindrical tubes with individual mean diameters. These diameters are measured and examined using the CAD-model as well as hands on measurements in the cylinder head. The diameters are then weighted as mean diameters using measurements at different cross-sections along the way from the inlet to the outlet of the ports.

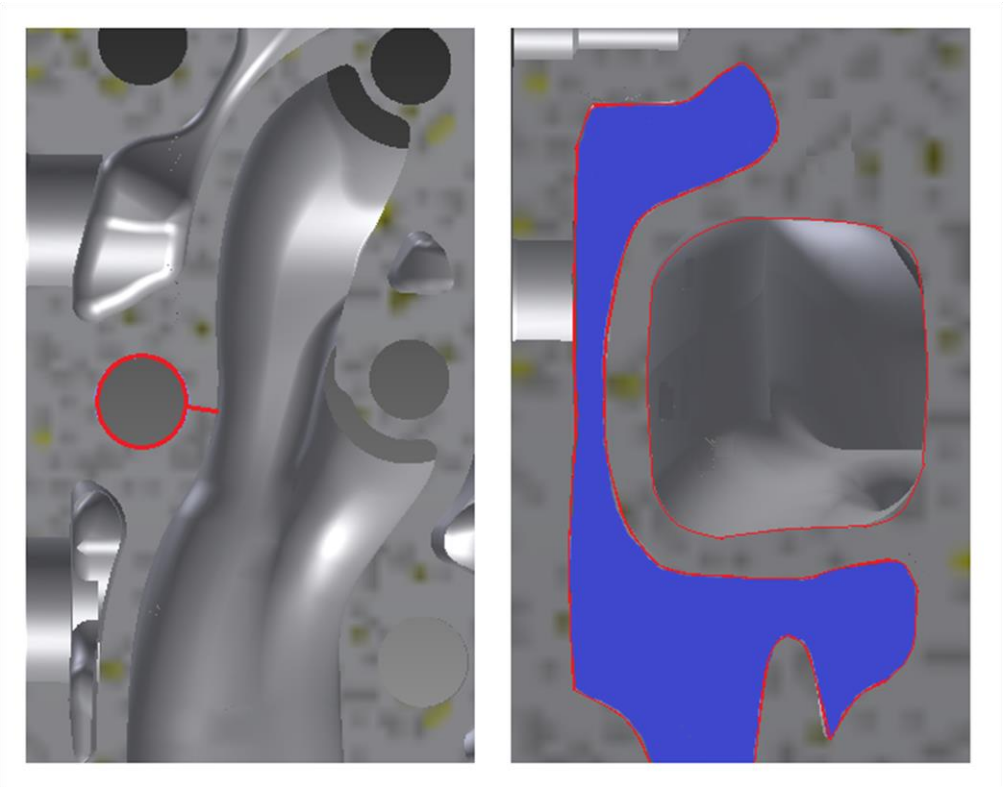

Figure 8 - Left: Perpendicular view of the distance to the bolt pillar. Right: Distance between the port and the water channel at a cross-sectional view 30 mm from the outlet [2]

4.3 Heat loss mechanisms

Heat transfer is driven by a net difference in temperature between two bodies. As of today, the process of this energy transfer only has scientific foundation to some extent. Consequently, some processes can be related to basic thermodynamics and fluid mechanics, while unknown processes are tackled by utilizing more empirically based methods from experimental results.

The transfer of energy from a higher- to a lower temperature body can occur through three different ways; *conduction, convection* and *radiation*. *Conduction* is related to molecular motion within a solid material or a fluid substance in a resting condition. In metals, the same phenomena is related to movement of free electrons in the material.

The process of *convection* is easier to grasp since it is based on macroscopic movement. This heat transfer occurs when fluids flow through or past solid bodies while a net temperature difference exists between the fluid and the solid material. Convection can be split into two different categories; forced- and free convection. In forced convection, the fluid motions are induced by external apparatus such as pumps and fans. In free convection, fluid motions are a result of local density variations.

Heat transfer through *radiation* is different in the sense that no medium is required in-between the emitting bodies, unlike in convection and conduction. In fact, heat exchange between two surfaces from radiation is at its maximum when there is no medium in-between. In radiation, energy is transferred at the speed of light through electromagnetic waves or so called photons, depending on chosen analysis theory (Maxwell's theory or Planck's hypothesis). All bodies emit thermal radiation and the total emitted energy is dependent on surface temperature and texture. As a result, some bodies emit more or less energy than others, even though the surface temperature might be the same [17].

[2] Closest distance to the bolt pillar is 5.829 mm, while the closest distance to the water channel is 5.923 mm.

4.3.1 Radiation

There is a measurement that quantifies the amount of incoming *radiation* to a given surface. A portion of this energy will transmit through the thickness of the body, another portion will be reflected at the surface of the body and the final portion will be absorbed by the body. The split between these paths can be illustrated with the following relation:

$$\rho + \alpha + \tau = 1 \tag{3}$$

Where, ρ = reflected portion, α = absorbed portion and τ = transmitted portion.

Most solid bodies do not transmit any radiation, these are called opaque bodies. In the simulations of the thesis, the insulating- and the conventionally used materials surrounding the gas mixture are both considered opaque, leading to the fact that $\tau = 0$. Because of this, equation 3 can be reduced to:

$$\rho + \alpha = 1 \tag{4}$$

The opaque casing will consequently absorb some of the radiation (α), which is considered a heat loss from the gas mixture due to irreversibility. The gas mixture will however receive some of the radiation back through reflection, along with the emitted energy from the wall or casing itself. These two separate products are additive and together they form the total *radiosity* (J) from the casing:

$$J = E + \rho G \tag{5}$$

Where G $\left[\frac{W}{m^2}\right]$ is the incoming radiation to the casing and E $\left[\frac{W}{m^2}\right]$ is the emitted radiation from the casing. Apart from the casing being opaque, one could assume that the same inner-casing is black due to soot forming from continuous exposure to exhaust remnants. The consequence of that would imply that no reflection occurs, i.e. that $\rho = 0$.

4.3.1.1 Radiation between gas and casing

With these prerequisites, the net heat exchange from the gas to the wall can be expressed as the emitted gas radiation minus the absorbed portion of heat emitted from the wall of the inner casing:

$$\dot{Q} = \left[\varepsilon_g(T_g)\sigma {T_g}^4 - \alpha_g(T_w)\sigma {T_w}^4\right] * A_{mantle} \tag{6}$$

Where $\varepsilon_g(T_g)$ and $\alpha_g(T_w)$ are the emittance factor dependent on the gas temperature and the absorbance factor dependent on the wall- and gas temperature, respectively. The emittance factor value ranges from zero to one and σ is the Stefan-Boltzmann constant, set to $\sigma = 5.67 * 10^{-8} \frac{W}{m^2 K^4}$ [17].

4.3.1.2 Radiation between casings

The radiative energy from a single body with surface area A can be determined using Stefan-Boltzmann's law:

$$\dot{Q} = \varepsilon\sigma T^4 A_{mantle} \tag{7}$$

Consequently, the energy that a body emits through radiation per area unit is a function of its temperature T and its emittance factor ε. Hence, the resulting radiative exchange will be the net difference between radiated energy from the body itself minus absorbed radiation from surrounding bodies. With regard to this, the net radiative energy between a hotter body (index 1) and a nearby colder body (index 2) can be calculated using:

$$\dot{Q} = \varepsilon_{res}\sigma A_1({T_1}^4 - {T_2}^4) \tag{8}$$

ε_{res} is a function of the two bodies' emittance factors, geometrical shape and their relative location to each other. In the simulations, the bodies that will interact with each other through radiative heat transfer are the inner and outer casings. ε_{res} for such a case can be calculated as:

$$\varepsilon_{res} = \frac{1}{\frac{1}{\varepsilon_1} + \frac{A_1}{A_2}\left(\frac{1}{\varepsilon_2} - 1\right)} \tag{9}$$

The used nomenclature is applicable to figure 9 below and is viable for any arbitrary shape of two areas facing each other. This is the case in the cross-sectional view of the exhaust ports with the two casings facing each other entirely. Hence, the total radiative heat loss can be calculated as [18]:

$$\dot{Q} = \frac{\sigma A_1}{\frac{1}{\varepsilon_1} + \frac{A_1}{A_2}\left(\frac{1}{\varepsilon_2} - 1\right)}({T_1}^4 - {T_2}^4) \tag{10}$$

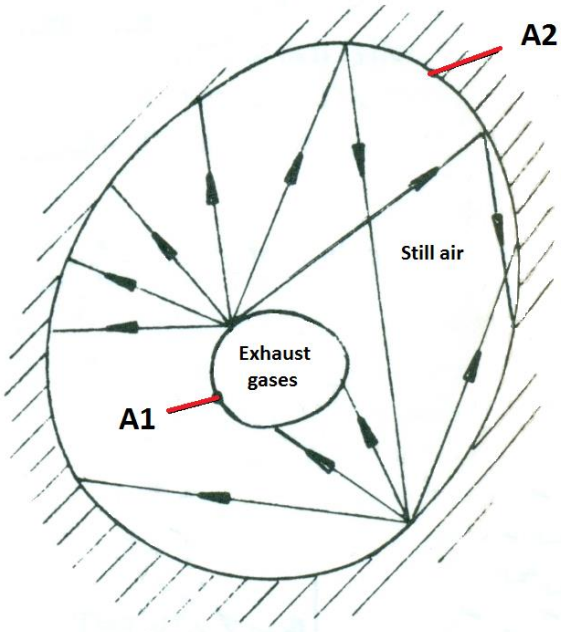

Figure 9 - Radiation between casings with area A1 and A2, with exhaust gases passing within A1 [18].

4.3.1.3 Assumptions and restrictions

The emittance ε_g from the gas depends on the composition of the gas mixture. However, apart from the gas mixture it has been shown that in-cylinder soot concentrations and the corresponding oxidation during combustion substantially affect the ratio of radiative to total heat transfer in Diesel engines. It has been reported that this ratio ranges from 11- to 40 % (in-cylinder conditions). In addition, the underlying reasons for the numbers and the complex dynamics are not fully understood as to date [19].

Due to software restrictions in predicting the concentration of the hot soot particles and their corresponding emittance contribution, quantitative results for radiative heat transfer between the exhaust gases and the inner casing will not be assessed or quantified in GT-Power.

For the radiative heat transfer between casings it is assumed that the surfaces are grey (non-black), i.e. that they are able to reflect radiation and that the emittance factors are general and hence independent on the varying individual wavelengths in the radiation. In addition, they are assumed to be diffuse, meaning that the radiative intensity is independent of the angles of radiation. It is further assumed that the casings are endless perpendicular to figure 9 and that both areas are fully exposed and visible to each other [17]. Values used for emittance factors are extracted from various lookup tables, depending on casing material properties. A complete list of parameters used in the simulations are presented in section 7.

4.3.2 Convection

The macroscopic movement of gas in relation to the casing materials at rest will heavily affect the convective heat transfer. In order to quantify such convection, the heat transfer coefficient $\alpha \left[\frac{W}{m^2K}\right]$ between the gas and the enclosing wall will have to be accessed. In this thesis, the enclosing wall or casing resembles a cylinder, and the material facing the gas will be composed of cast iron during the first round of simulations and steel material during the second round. The different materials will have different surface roughness values, resulting in different values of α for the different materials.

The speed of the gas bulk mixture (u_m), derived from the mass flow, is used in GT-Power in order to determine various flow characteristics, e.g. if the flow is laminar or turbulent. If simultaneously the diameter of the port is known (D), as well as the viscosity of the gas mixture (υ), the Reynolds number can hint the flow characteristics according to:

$$Re = \frac{u_m D}{\upsilon} \tag{11}$$

For pipe flow, the laminar flow becomes unsteady around $Re \approx 2300$. With knowledge of the Re-number as well as the roughness of the material, denoted $\varepsilon[m]$ in this section, it is possible to predict the friction factor f using the Moody-chart in figure 10, which is graphical representation of the empirical and adapted Cole-brook formula. For turbulent flow situations, one can adequately approximate this formula into the Haaland equation, granting the benefit of explicitly determining the friction factor without any iterative process:

$$\frac{1}{\sqrt{f}} = -1.8log\left[\left(\frac{\epsilon/D}{3.7}\right)^{1.11} + \frac{6.9}{Re}\right] \tag{12}$$

The transition range from laminar to turbulent flow can be seen in the Moody chart in figure 10. Hence, Haaland's formula is valid after the transition area ($Re > 3000$) and for round pipes [20].

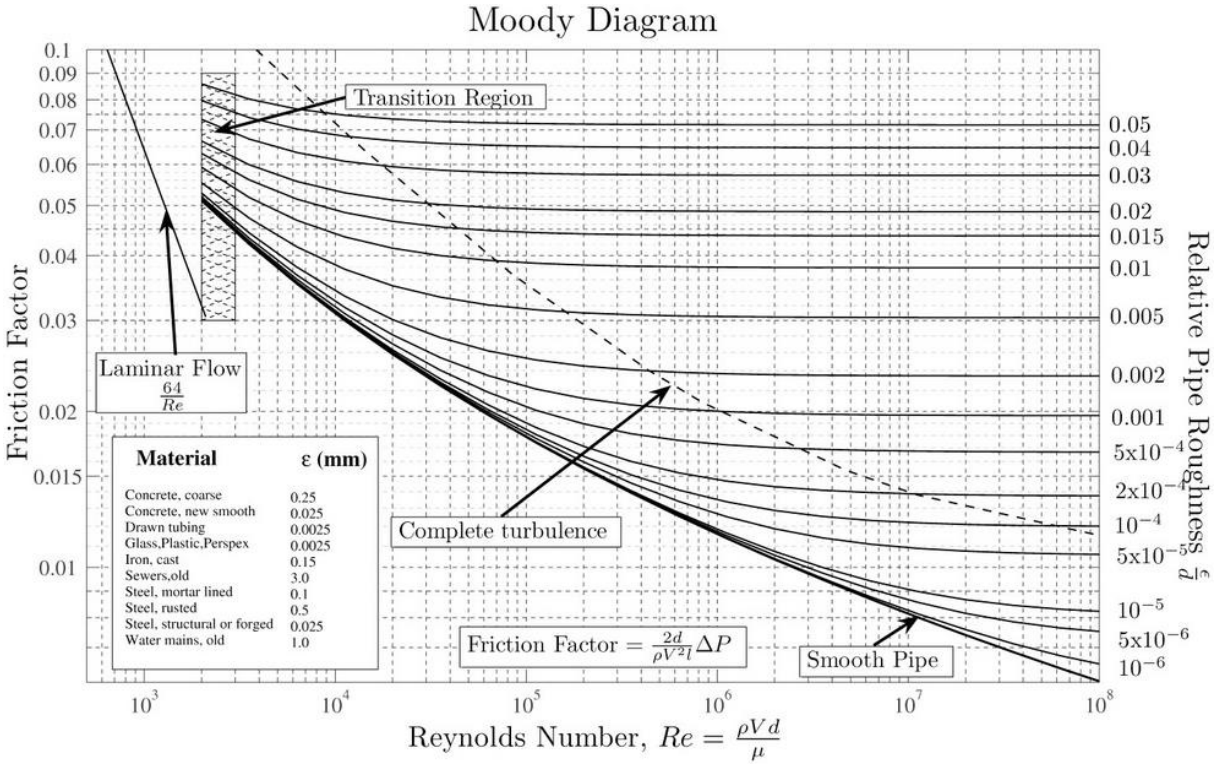

Figure 10 - Moody diagram [21]

Hence, with knowledge of the Re-number, surface roughness and pipe diameter, it is possible to determine the friction factor f. Finally, the convective heat transfer coefficient α can be determined with the *Reynold analogy* according to equation 13, where U, c_p and ρ are the bulk speed, specific heat and density of the exhaust gases, respectively [17]:

$$\frac{\alpha}{\rho c_p U} = \frac{f}{8} \tag{13}$$

In GT-Power, this α coefficient is used in conjunction with the surface area inside the pipe and the temperature gradient between the average gas bulk temperature and the registered wall temperature in the middle node of the wall. Consequently, the total convective heat transfer is calculated according to equation 14:

$$\dot{Q} = \alpha\left(T_{gas\ bulk} - T_{mid\ wall}\right)A_{mantle} \tag{14}$$

4.3.2.1 Assumptions and restrictions

The convective heat transfer process in GT-Power is closely transparent to the fundamental heat transfer theory outlined in the section above. However, some restrictions are introduced in the model that are not entirely in line with the future setup in practice. For example, each port is individually connected to one valve each in the model, meaning that the flow is split between two separate channels. In reality, the exhaust gases from each port are able to interact with each other from the moment of discharge from the exhaust valves. This complex interaction will most likely produce different flow dynamics and hence different heat transfer coefficients than those generated from individual and closed off channels like in the GT-Power model.

The heat transfer coefficient in equation 14 is assessed in GT-Power using the described methodology in section 4.3.2. However, the heat transfer coefficient between the outside of the last layer and the

water channel is set to a constant input value derived from a lookup table. Hence, no fundamental flow analysis is done in the outside water channel.

4.3.3 Conduction

Once the heat is transferred from the gas mixture to the wall casing of the cylinder, the conductive heat transfer will dissipate heat radially through the different enclosing layers. In the initial simulations, there will only be one such layer made out of conventional cast iron. In the second round of simulations, additional layers will be added with the goal of decreasing the conductive heat transfer. Regardless of the layer setup, the fluid surrounding the outer and final casing will constitute of cooling water, with an average and close to constant temperature of $T_{cooling\ water} = 95$ °C.

In similar analogy with convective heat transfer, the total conductive heat transfer through a solid material is described using the temperature gradient between each endpoint of the solid's walls, as well as the characteristic area participating in the heat transfer. In addition, the conductive heat transfer is also a function of the thickness of the material. Ultimately, this introduces a new metric dimension that consequently affects the dimension of the heat transfer coefficient, denoted $\lambda \left[\frac{W}{mK}\right]$.

$$\dot{Q} = \lambda(T_{inner\ wall} - T_{outer\ wall})\frac{A}{t} \tag{15}$$

In equation 15, $T_{inner\ wall}$ is the temperature of the wall closest to the exhaust gas mixture, while $T_{outer\ wall}$ is the lower temperature directly facing the cooling water [17].

4.3.3.1 Assumptions and restrictions

The quantification of conductive heat transfer is derived from the construction of different layers enclosing the exhaust ports. Hence, the output is reliant on correct inputs for parameters such as the thickness of layers as well as material properties such as specific heat, density and conductivity. For optimal results, material properties that vary with operating conditions should be provided to GT-Power as functions of different temperatures. In theory, longer array lists are more accurate and should yield better results. However, lack of comprehensive lookup tables resulted in limited input, which could potentially affect the results. Nevertheless, simulations showed that the magnitude of these lookup tables had little effect on the final results.

The cooling water circulating the exhaust ports is assumed to keep a constant temperature of 95℃. It is further assumed that the water channel covers the entire channel at a fixed radial distance. This leads to the assumption that the water temperature will affect the radial temperature gradient in each node of the modeled exhaust ports.

5 CFD Analysis

With CFD analysis, one can predict the flow velocities through the exhaust ports. This is informative from a heat loss perspective since flow velocities will greatly affect the convective heat transfer according to *Reynold's analogy.*

The valve seats, running through the white dots in figure 11, induce high velocities caused by their relatively sharp and irregular edges, generating enhanced turbulent behavior through local pressure drops and flow acceleration [20]. This consequence can be seen clearly in the upper right picture, displaying increased flow velocities around the seats. The valve opening in the same picture is set to 6 mm and is defined as the vertical travel length from the closed position (displayed in the bottom right picture).

High velocities can also be seen in the "throat" section where the right and left port channels merge. This turbulent interaction is clearly visible in the upper left picture, where the valve opening is at 2 mm. In the bottom left picture, high velocities can be seen along each side of the wall. As a suggestion, this is caused by the combination of a small cross area, local increase in mass flow (from the merging of gases from each port) as well as the rather aggressive geometrical turn at each side, changing the flow angle of the exhaust gases in short time and distance [20].

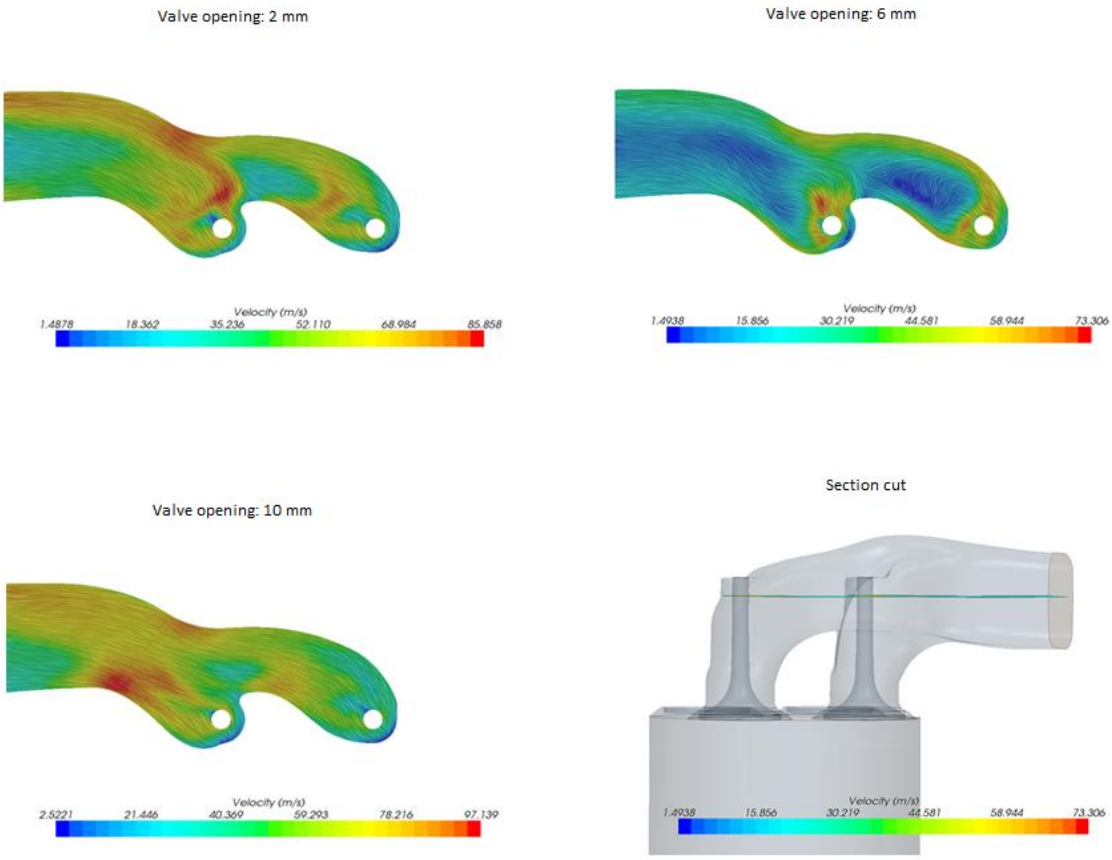

Figure 11 - Flow velocities through the exhaust ports with varying valve openings

6 Insulating materials and applications

The transportation of heat through solid materials is dependent on lattice vibration waves (phonons) and free electrons within the material. The lattice vibrations can be explained as the elastic vibrations between arrangements of atoms, transferring thermal energy in the direction of their motion. These vibrations, together with the contribution from free electrons, determine the total thermal conductivity of the solid.

Metals are commonly known to be great thermal conductors. This is due to the relatively large amount of free electrons that contribute to higher thermal conductivity. Hence, the relative contribution from lattice vibration waves to the total thermal conduction is small in metal solids. The highest total conductivity come from high-purity metals, while the conductivity is reduced when impurities are introduced, e.g. when the metals are alloyed. These impurities act as scattering centers, which ultimately impairs electron movement and consequently reduces thermal conductivity, creating insulating properties [22].

Insulating materials within combustion engines rose in interest during research of the Low Heat Rejection Engines (*LHRE*). Due to the harsh environment within the engine, it was established that in order for these insulating materials to be feasible, they must have high temperature strength, suitable expansion coefficients, low friction characteristics, light weight, good thermal shock resistance and durability [23]. In addition, they must be characterized with having low thermal conductivity [16].

Polymers can reach low thermal conductivities, but they lack thermal resistance, especially due to low melting temperatures. Compared to metals and polymers, suitably engineered ceramics are capable of providing the mentioned criteria to a higher extent, making them strong material candidates for insulation in harsh environments such as within exhaust ports of combustion engines [22].

6.1 Ceramic insulation

Ceramic materials lack large numbers of free electrons. The main thermal conductivity is instead caused by lattice vibration waves, which are not nearly as effective at transporting heat energy as the free electrons. Consequently, thermal conductivity is relatively low when compared to metals.

The lattice vibrations are affected by temperature. For most ceramics, the thermal conductivity decrease as temperature increases, as can be seen in figure 12. The eventual increase in thermal conductivity is caused by an increase in radiant heat transfer from the environment.

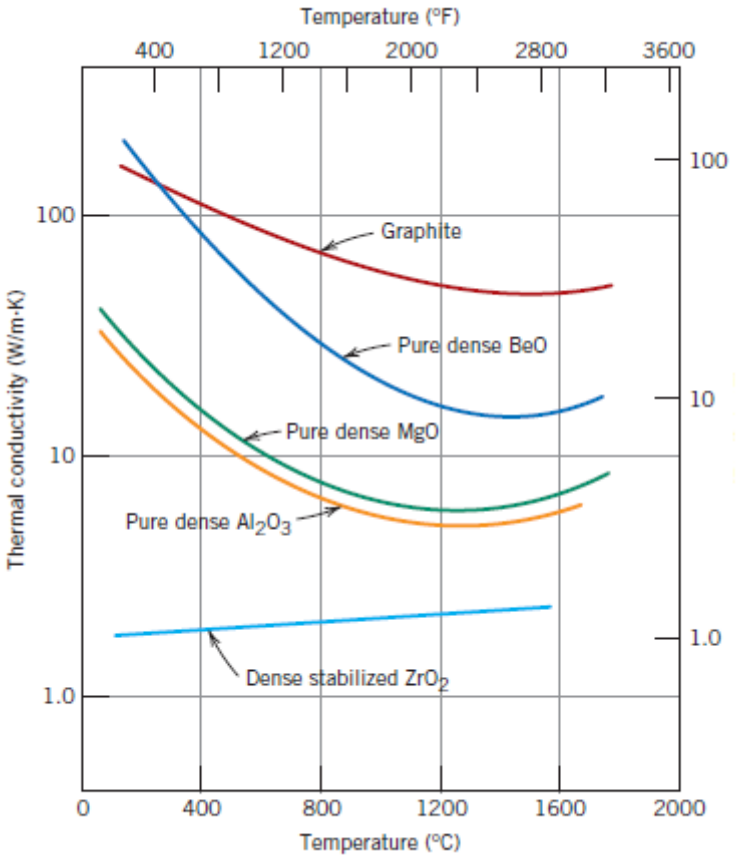

Figure 12 - Thermal conductivity for a selection of arbitrary ceramics as a function of temperature [22].

As can be seen in figure 12, Zirconia (ZrO_2) looks attractive from a conductive point of view. In addition, Zirconia has showcased good strength and higher temperature resistance than most metals, while simultaneously keeping thermal expansion coefficients close to metals, reducing the likelihood of detrimental interfacial stress. From a drawback point of view, Zirconia exhibits phase changing with increasing temperatures. In an effort to bypass this phase changing, Zirconia is often altered into Partially Stabilized Zirconia (PSZ).

In order to decrease thermal conductivity even further, ceramic materials with distinct porosity are often utilized. The pores act as small volumes of thermal barriers, since they are usually filled with still air that has very low thermal conductivity. In addition, the pores introduce the heat transfer mechanic of convection, since the ceramic material must interact with still gases in the pours in order to progress. This gaseous convection with still air is very ineffective, granting additional insulating benefits [22].

6.2 Practical applications of insulation

This section highlights previously tested applications for insulating purposes. Most of the prior research to date have been concentrated to in-cylinder applications, motivated by the philosophy of Low Heat Rejection Engines (*LHRE*). However, this section examines the possibilities of transferring in-cylinder research, like material usage and application procedures, to the exhaust ports. This could potentially be done in an easy manner or through minor modifications of the ideas. In addition, conducted research that specifically targets the exhaust ports will also be presented.

This section can be viewed as a screening of potential applications. Hence, some ideas might seem unrealistic, but they might fulfill a purpose of stimulating new ideas through innovative and "out of the box" thinking.

6.2.1 Case 1 – Tight casting with premade casing

From a production point of view, it would be beneficial if the ceramic insulation and the conventional cylinder head could be fully merged during regular casting of the cylinder head. This insulation could constitute a single layer between the exhausts and the base metal of the cylinder head, or the same setup but with the addition of an inner casing facing the exhausts if protection of the insulating material is required. Either way, the insulation must be able to withstand the thermal shock and high temperature from the initial casting process, reaching temperatures of around 1420 °C. In addition, hot liquid metal from the casting process must not enter and alter the insulating material [24].

During casting, the inner casing or ceramic material will be supported by a sand core in order to provide stabilization in the channels and against the valve seats. The final product, using a protective casing, can be visualized in figure 13. The benefit of using the protective casing is the ability to glue insulating blankets made out of e.g. ceramic fibers onto the casing. In addition, the protective casing can be engineered with better surface roughness compared to the insulation. Another benefit is that the casing may act as a protective barrier, hindering ceramic particles from detaching and entering the combustion chamber. The proposed setup in figure 13 would also imply an altering of the traditional shape of the port, being more rectangular due to a trade-off between flow and the available space for the bolt pillars in the cylinder head. The choice of using a cylindrical shape is related to load-bearing properties, especially since ceramics in general are not very ductile and thus subjected to increased probabilities of experiencing fractures, especially if there are sharp edges in the design [25].

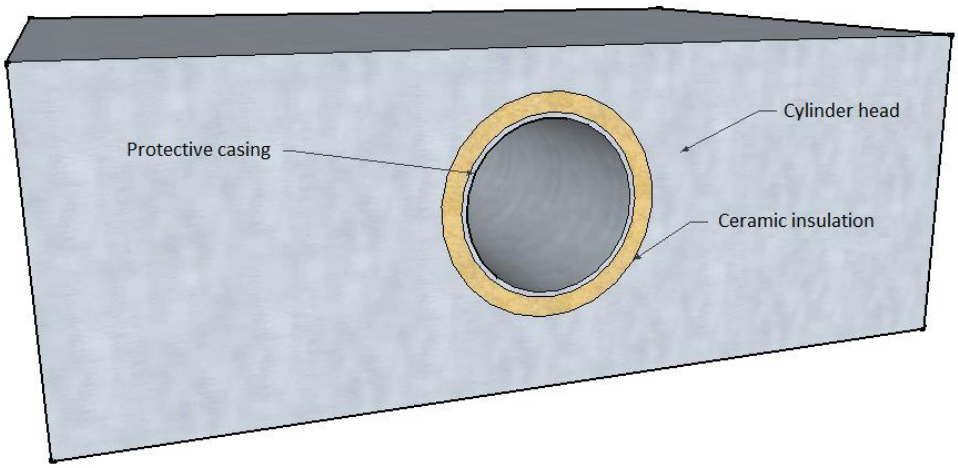

Figure 13 – Proposed casting with optional protective casing

Experiments similar to this case have been conducted. In one specific approach, a cylindrical casing made out of stainless chrome steel ($SS2300$) was used inside the exhaust ports. On the outside of that casing, an insulating material made out of fiberglass and aluminum oxide was glued onto the surface like a blanket around the casing. This arrangement was then enclosed during the casting process of the cylinder head, where the melting point between the cast iron and the insulation only differed by approximately 10 °C. Hence, just enough to avoid the hot iron from decomposing the insulating material around the metal casing.

Running the engine at full load with this setup indicated a redistribution of power between the cooling water (reduction) and the exhaust gases (increase) by approximately 8.4 %. However, post-examination of the ports revealed problems with insulation leakage and also cooling water leakage that could be traced to the required altering of the cylinder head geometry in order to fit the entire insulation arrangement. A smaller amount of the insulation had also detached from the chrome steel casing due to stronger adhesion to the iron molding at certain points. This can be solved with so called blacking procedures which alters the adhesion [24].

A problem with this case is that the used materials often have different thermal expansion coefficients, leading to different movements in the interlayers during casting. This often results in cracking of the ceramic layer. To prevent this, it is possible to use silicate spheres or other flexible inserts along the interlayer, with the dedicated task of absorbing the shrinking force from enclosing layers [24]. Using elastic spheres along the interlayer also allow remnant gases from the slightly decomposed ceramic fibers, induced by the hot iron mold, to be able to escape the ports. Otherwise, these gases might expand locally and cause cracks [25].

6.2.2 Case 2 – Tight casting without casing

The complex geometry of the exhaust ports severely complicates the application of pre-casted ceramics, especially without inner casing support. However, there are reports from successful attempts that also indicate a significant decrease in heat losses to the cooling fluid. In one experiment, casted exhaust ports made out of aluminum titanite (Al_2TiO_5) were successfully casted into the cylinder head, without the usage of inner casings. This action led to a 10 % reduction of energy flow to the cooling fluid, which was instead redirected to the exhausts. However, this redistribution could not be fully attributed to the insulating procedure.

Once again, the contraction difference between the aluminum titanite ports and the iron mold due to different thermal expansion coefficients caused problems. After casting, the iron mold shrunk to a higher extent, which resulted in cracking of the aluminum titanite ports. In order to mitigate this, elastic silicate spheres were put in the interlaying space in an effort to absorb the induced tensions. However, post-examination of the ports still revealed cracks, although smaller when thicker layers of silicate spheres were used [24]. The basic setup for this case and the corresponding experiments can be seen in figure 14.

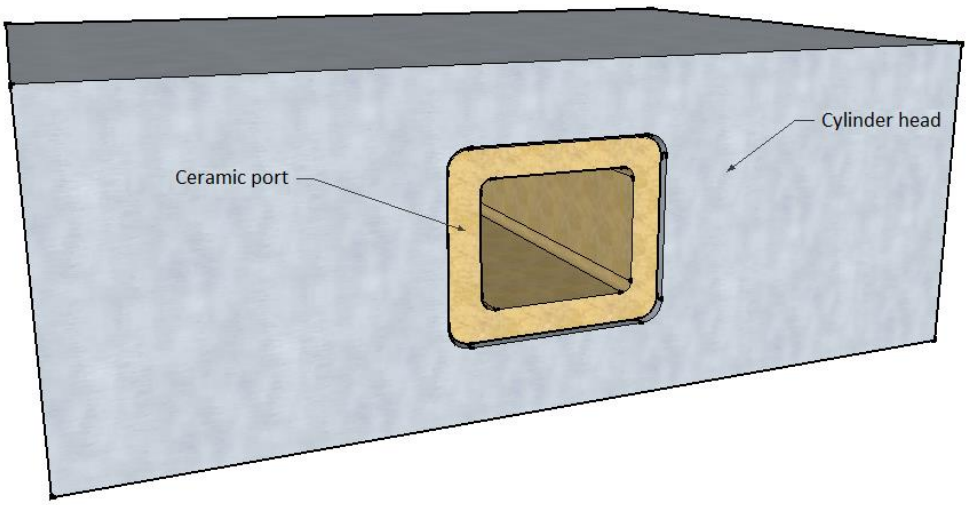

Figure 14 – Casting an insulated port without inner casing

6.2.3 Case 3 – Ceramic filling or air gap

This alternative is similar to the conventional and more rectangular exhaust ports, with the addition of utilizing a supportive casing. The reason for having the casing is now mainly based on the need for a supporting wall as the void between the cast iron mold and the casing is to be filled with an insulating fluid/solid. With this setup, one could still utilize the ceramic fiber blanket for filling the void. However, with a more rectangular and irregular geometry of the port, it might be difficult to get an even distribution and thickness all around the protective casing, while simultaneously keeping a tight fit to the surrounding cylinder head. Figure 16 gives an idea of the case, before filling.

6.2.3.1 Ceramic filling

Filling the void could be achieved as a post-casting process. However, before filling it is important to investigate that there is no possibility for the filling to escape the ports and enter the cylinder. Hence, there must be a complete connection between the cast iron mold and the inner casing all the way back to the valve plates. In order to cast this, two sand cores must be used. One core for the inside of the casing, and one core between the casing and the iron mold. The sand must also be successfully withdrawn after casting in an efficient manner. Regardless of the chosen filling, the final setup can be visualized in figure 15.

This type of setup is not very attractive from a production point of view, as it introduces many complications. First of all, the design now has two interfaces that must be aligned in terms of thermal expansion rates. In addition, practically every method for casting ceramics results in significant shrinkage. This shrinkage can easily reach around 25 % during the drying phase of the ceramic part, creating huge tolerance issues. Also, still air is able to generate similar values of conductive heat transfer as the potential ceramic filling [26]. If air is utilized in the void instead, there is no material cost and the problems with tolerances, shrinking and cracking disappears [25].

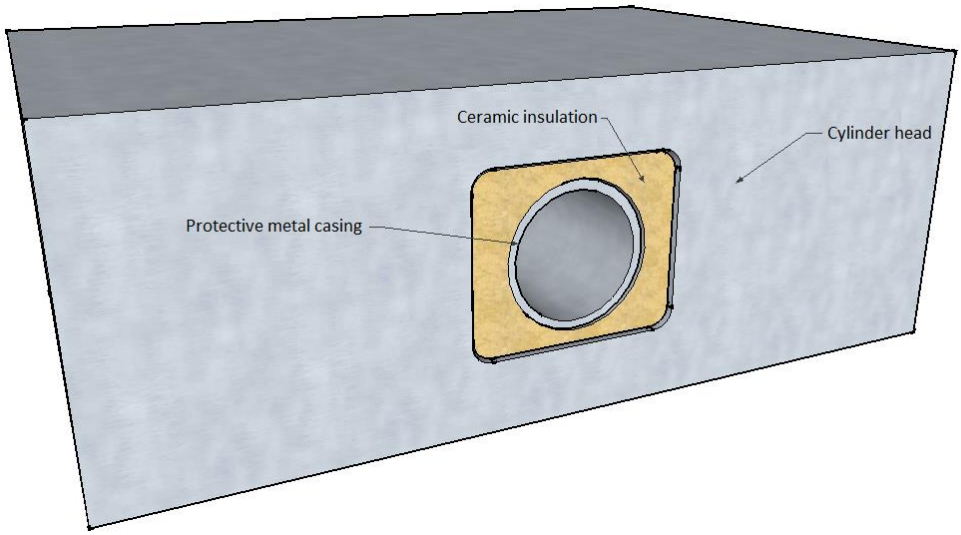

Figure 15 - Proposed casting with optional protective metal casing

6.2.3.2 Air gap

Having air in the void between the casing and the cylinder head eliminates most of the problems described in the section above. Instead, the final setup would have a design according to figure 16. However, the manufacturing of this port would still require separate sand cores for each void, inside and outside of the protective casing. As in the previous setup, it is important that there is full closure at the attachment between the cylinder head and the inner casing, i.e. that no exhaust gas is able to flow across the space of still air between the inner casing and the cylinder head. This would defeat the

purpose of using still air as insulation since leakage and hence increased flow would increase the convective heat transfer. The attachment point of the casing must also be sturdy so that the casing doesn't oscillate as the exhaust gases travel through it periodically. This might cause problems with mechanical strength and potentially even efficiency, since power is lost putting the casing into oscillation instead.

A benefit of this design is that the heat transfer coefficient between the inner casing and the still air will be very low due to natural convection from the air at rest. In addition, the heat that dissipates to the air will travel very inefficiently across the air layer due to the fact that still air has a thermal conductivity of around 0.02 $\frac{W}{mK}$ [26].

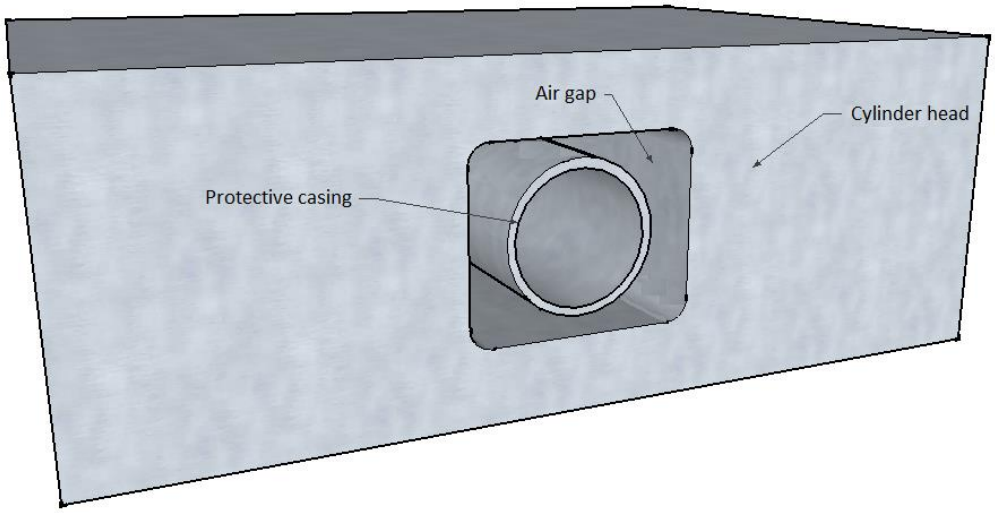

Figure 16 - Proposed casting with air gap and protective casing

6.2.4 Case 4 – Thermal barrier coating

As stated, different material properties between conventional cast iron and insulating materials have caused problems during the casting process. As a consequence, solutions have been sought that do not require simultaneous casting and merging between different solids and insulating materials. Instead, conducted research has examined the effect of so called thermal barrier coating. This coating procedure is a post treatment process, carried out on already manufactured parts such as exhaust ports. The coating treatment is proven to successfully reduce wear and abrasion failure in high temperature engine applications, as well as reducing heat dissipation through the same material.

During the 70's, silicon carbide (SiC) and silicon nitride (Si_3N_4) were used extensively for engine insulation research. The materials exhibited good wear resistance, low friction coefficients, great temperature capabilities and good corrosion resistance. Unfortunately, they fell short due to brittleness and shrinking behavior during sintering, motivating a hunt for new materials [27].

6.2.4.1 Spraying approach

According to experimental studies conducted by A.J Modi, a conventional four-stroke, twin cylinder and water cooled diesel engine showed not only reduced heat losses to the cooling system, but also reduced fuel consumption when thermal coating was applied within the cylinders. In the experiments, a modified conventional engine was coated with Partially Stabilized Zirconia (PSZ), using $NiAl$ as bond coat. The coatings were applied to the combustion chamber valves, piston crown faces and liners. A.J Modi concluded that the exhaust energy increased by up to 24 % with insulation coatings as prescribed

in the two cylinders. Similar experiments conducted by Prasad and Samria showed a 19 % reduction in heat loss through the piston itself when the piston crown face was coated with Partially Stabilized Zirconia. Figure 17 shows the piston crown and the depth of each coating layer applied in the experiments [27].

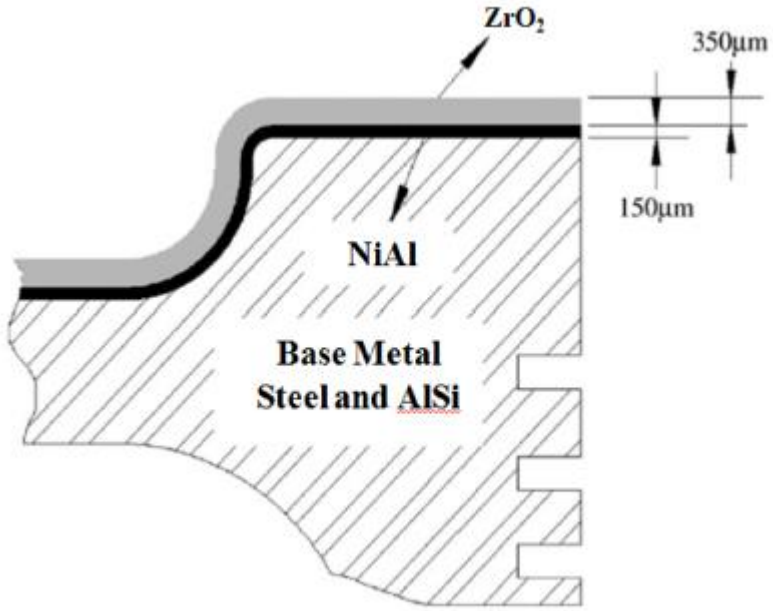

Figure 17 - In cylinder coating depth used by A.J Modi [27]

Various experiments similar to the ones conducted by A.J Modi have also been conducted, using different bond coats and chemical rectifications. Other examples of coating combinations that also showed decreased heat rejection are ZrO_2-Al_2O_3, ZrO_2-Y_2O_3 and ZrO_2-$NiCrB$ [28]. However, all of these experiments were concentrated to the cylinder of the engine, meaning that there is a gap in research regarding the practical application of thermal barrier coating to the exhaust ports. However, FEA (Finite Element Analysis) on the exhaust ports, followed by practical experiments on a LHRE were conducted by Bing, Yong and Meilin. Their simulations showed that when the exhaust ports were insulated with ZrO_2 the heat transfer through the ports decreased by 13.2, 14.9 and 18.2 %, using coating layers of 0.7, 1.0 and 1.5 mm respectively. Hence, it was concluded that the heat transfer decreased with increasing coating layer thickness [29].

Partially Stabilized Zirconia (PSZ) is by far the most researched ceramic for insulating purposes. It stands out from the other ceramics due to the fact that the thermal expansion coefficient is very close the corresponding coefficient of cast iron. In addition, it's characterized by having low thermal conductivity. Table 6-1 shows expansion coefficients and thermal conductivity for a selection of different materials used in coating applications, including materials used as bond coat additives.

Table 6-1: Expansion coefficients and thermal conductivity for solids commonly used for coating applications, compared with the corresponding values for cast iron, onto which they merge

Material	Thermal Expansion Coefficient $\left[10^{-6}\ \frac{m}{mK}\right]$ [30]	Thermal Conductivity $\left[\frac{W}{mK}\right]$ [26]
ZrO_2	10.5	3
PSZ	9.8	2.5
Si_3N_4	3.2	12
Al_2O_3	7.7	32
Y_2O_3	7.2	5
$Cast\ iron$	10.8	46 [31]

Different additives have been applied to PSZ in order to increase ductility and strength characteristics, like e.g. Magnesium and Nickel. There have also been experiments where the coating order was reversed in comparison to experiments by A.J Modi (figure 17). Instead, a so called densification process was conducted, where applied PSZ was coated with chromium oxide (Cr_2O_3), filling up the pours in the PSZ. This treatment showcased 87 % lower wear rate than the case without densification treatment [16].

One of the main issues with thermal barrier coating is associated with reachability. Applying it to liners, piston crown faces and valves is one thing, since these components can be processed and applied to the cylinder head individually. However, it is more difficult to apply coating to an enclosed and tight space that is molded in place, like the exhaust ports. Hence, the coating torch is limited to a certain depth of practical application inside the ports.

6.2.4.2 Alternative approach

One idea is to apply thermal coating directly to the sand cores that are to be applied in the exhaust ports before casting. The diameter of the sand cores could be reduced by the equivalent layer thickness of the proposed coating. When the sand is extracted, the fixed coating will remain, forming a part with the geometry of an exhaust port. However, there is a risk that this design is inferior from a robustness point of view since there is no solid metal support what so ever. The part will most likely be very brittle and dynamic movements during load such as vibrations may pose a threat to the survivability of this design. In addition, it is unclear if it can withstand being molded into the cylinder head. Figure 18 shows the part after the sand has been withdrawn, with visible traces of sand grains along the rough surface.

Figure 18 - Coating applied directly to sand core surface

6.2.5 Case 5 – Applying insulating inserts

An alternative to casting- and coating solutions is the insertion of ceramic parts after finished casting of the cylinder head. Such a solution was applied in conducted experiments by Louki and Peters, where a Nimonic 80A insert was put in the aluminum piston of the engine. This casing was capable of withstanding temperatures of around 1080 K [32] and provide better insulation than the conventional aluminum. It was shown that the insertion managed to increase the piston's wall temperature by approximately 250 Kelvin, up from the original temperature of around 500 Kelvin. From this, it was concluded that the insert managed to contain the energy in a more efficient manner compared to the conventional setup [15].

In the previously mentioned experiments by Yong, Bing and Meilin, a metallic insert was used for supportive purposes in the exhaust ports. This decision was based on the poor flexibility of the ceramic coating in conjunction with high mechanical- and thermal stress during engine operation. If the coating would break, they feared that material would enter the cylinder and alter the operation of the engine. As a solution to this possible event, a heat-bearing layer made out of $CrNi_{18}Ti_9$ was added, forming a protective barrier that held the coating in place [29].

For the exhaust ports, one suggestion is to glue ceramic fibers around a supportive casing. In addition, if the ceramic fibers are sensitive to the heat from the upcoming casting process, an optional protective casing can be added outside the ceramic layer, forming the setup visualized in figure 19. Regardless of the chosen design, the overall thickness and final diameter of the insert will put a constraint to the ability of insertion. Hence, there will be a tradeoff between the required diameter for the flow, required protection (protective or fixating casings) and the maximum allowed diameter for satisfactory insertion reach.

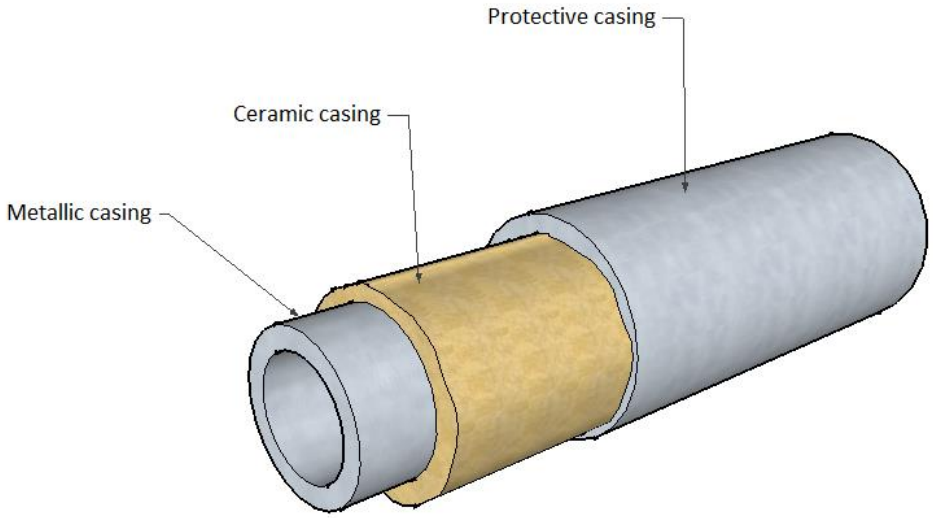

Figure 19 - Proposed insert with optional ceramic- and protective casings

Regardless of the setup, there will be inevitable local gaps between the insert itself and the cylinder head due to several points of misalignment. This is not necessarily a bad thing, since it will generate smaller pockets containing still air, generating the same effect of low heat transfer that was discussed in section 6.2.3.2. Figure 20 visualizes the resulting air gap between the casing and the cylinder head after complete insertion.

Generally, thinner inserts will be able to reach further into the exhaust ports. If e.g. length is a high prioritized criteria, the design from figure 19 could be reduced to the metallic casing only, motivated by the fact that the casing itself has lower thermal conductivity than the cast iron in the cylinder head. This would imply greater length coverage inside the exhaust ports, but also larger air gaps closer to the outlet since exhaust ports generally narrow as the distance to the valves shortens. This could potentially be avoided if the cylindrical insert design is abandoned, e.g. if the insert's geometry is semi-cylindrical instead.

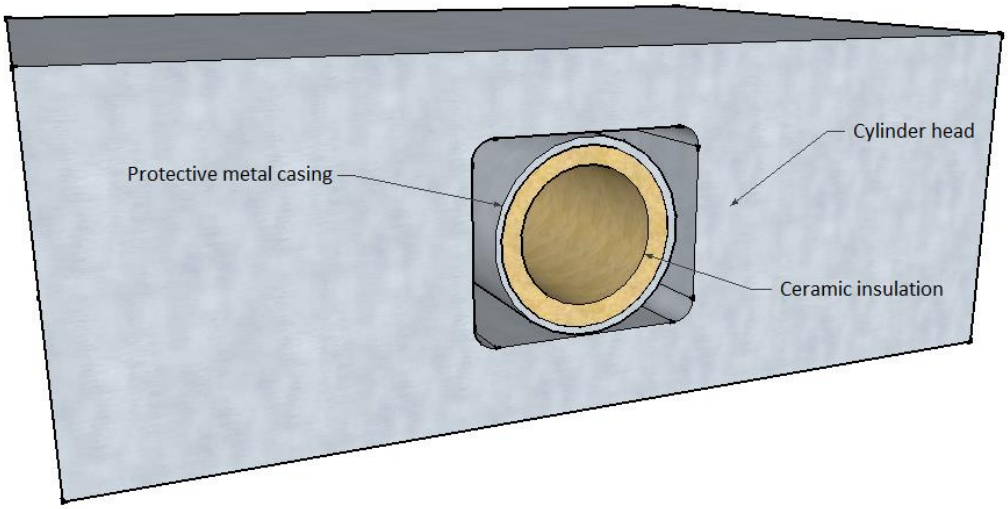

Figure 20 – Basic illustration of an insert in place, without an inner metallic casing

The metallic insert used in figure 20 can be constructed by utilizing the theory of different thermal expansions between different materials. More specifically, the metal casing can be expanded in diameter by undergoing a heating process. Followed by the heating, the casing can be slid over and mounted around the pre-casted ceramic insulation. The subsequent cooling will cause the metal casing to shrink, ensuring a tight fit between the two materials. However, if the insulation works as intended, it will be heated to a higher extent compared to the surrounding metal casing due to better containment of energy. Hence, with poor tolerances and wrongly chosen materials, the ceramic insulation might expand more than the metal case and potentially crack the ceramic itself or the metal casing due to increased stresses in the interlayer. Consequently, a cylindrical design is preferred for better load-bearing capabilities in the likelihood of this described event [25].

6.2.5.1 Applying the insert in practice

One of the major limitations of using inserts is connected to reachability and the ability to properly fixate the insert. As the insert is often used post-casting, the reach is bound to the geometry subjected to the application, e.g. the exhaust ports. Figure 21 demonstrates such practical limitations directly coupled to the exhaust ports that are to be used in following experiments. The figure displays two different cylindrical casings with different diameters. As can be seen, each insert will require smaller modifications to the existing cylinder head as the edges reach past the original exhaust port geometry. However, these modifications are within a reasonable range, avoiding potential entry to the surrounding water channel and manipulation of any bolt pillars.

Another problem with the two inserts is related to alignment. From this perspective, the shorter casing is well fitted in the port, meaning that the flow from each channel won't escape around the outside of the casing. This event would trap exhaust gases further downstream where alignment is achieved,

creating a recirculating effect. Additionally, the inserts must not have bulky edges that can directly obstruct the flow. This would most likely induce turbulence and hence increased convective heat losses, reducing the efficiency of the insulation method. This particular situation might occur for the second casing in figure 21 (colored in green). As can be seen, the insert reaches further into the channel, but it will not be able to efficiently catch the complete mass flow from the left port. Instead, it will act as an obstruction to the flow, causing more harm than good to the overall heat transfer. Nevertheless, it is realistic to assume that roughly 10-25 % of the wall area in the ports could be covered with the usage of inserts, judging from figure 21. This ultimately renders the insulation method significant from a coverage point of view, despite its application problems.

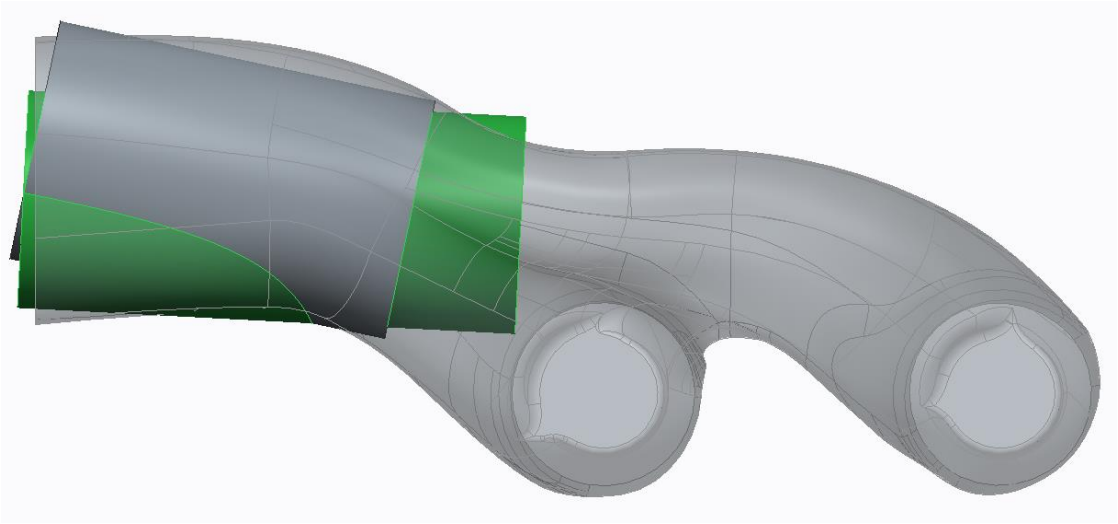

Figure 21 - Depth illustration of different inserts

6.3 Chosen case for application

Upon consultation with manufacturing parties, it was made clear that tight casting and the application of inserts were viable options considering the time schedule for the experimental rollout. However, tight casting had the upper hand due to the ability to completely cover the complete area within the ports [33] [25].

Filling procedures that required simultaneous casting of ceramic insulation and conventional cast iron were dropped due to severe tolerance issues caused by shrinkage. Additionally, thermal barrier coating was considered too taxing when considering the application effort needed in relation to the potential reduction in heat transfer. As described, the coating procedure also falls short as an application candidate for the exhaust ports due to reachability constraints.

The remaining alternatives consisted of tight casting with or without supportive/protective casing, represented by case one and two. There was also the possibility to go for case three, utilizing air as filling for the void. However, since the *DCEE* concept is designed to run at elevated temperatures compared to traditional concepts, it was unsure whether the air gap would cause too high radiative heat transfer. Especially if the combustion reaches stoichiometric conditions, which is planned in future experimental research of the concept.

The final decision was made to go for case one, using ceramic fibers as insulation. The chosen material consisted of saffil alumina, having good thermal resistance as well as a competitive conduction coefficient ($0.2\ \frac{W}{mK}$). These ceramic fibers are incorporated into blankets that are flexible enough to be bent and fitted around e.g. cylindrical geometries. Naturally, this approach enables fitting of the

ceramic blanket around a supportive casing, using e.g. glue. After complete application, the setup would look something like the one depicted in figure 13.

The saffil alumina blanket is resistant to significant shrinking behavior during heating/cooling and is capable of withstanding the thermal shock from the casting process relatively well. In addition, the application is a workaround from casting directly against brittle ceramic parts, subjected to cracking due to missing flexibility. However, some tensions will still arise between the cast iron and the ceramic blanket due to differences in thermal expansion coefficients. According to the manufacturer, this potential mismatch will not be significant, meaning that the insulation is capable of providing required elastic ductility, acting as dampening in order to avoid cracking or rupturing of the insulation.

Apart from elastic dampening, there is yet another problem linked to the casting process that could potentially cause rupturing of the insulation, i.e. expansion from gas remnants. The high temperatures will unavoidably decompose smaller fractions of the insulation, generating local gas remnants in the process. This gas must be able to continuously escape the ports during casting. If not, the gas will expand locally and potentially rupture the insulation. In order to avoid this, small holes will have to be made and distributed along the metal casing, using e.g. laser puncturing. This will enable escape routes for the gas, but also for the heat that is able to dissipate radially through the holes, bypassing insulation. Naturally, this is an unwanted effect, but a required action in order to follow through with successful casting [34].

7 GT-Power simulations

The exhaust ports are modelled as cylindrical channels with varying length. Consequently, the heat transfer will be dependent on physical characteristics connected to the flow in such geometries, as well as material- and gas properties inside, through and outside the channels. The following sections in this chapter will present global parameters and assumptions that are common to all simulations, independent on whether conventional- or insulated ports are examined.

The initial simulations will study sweeps with varying port diameters of the conventional exhaust ports. These simulations are followed by sweeps of insulation thickness coupled to the chosen insulation case. These simulations will be based on the optimal flow diameter from the initial simulations. The final simulations will focus on maximizing peeling of the water channel- and cast iron thicknesses, focusing on enabling maximum space for insulation thickness while maintaining a minimum allowed thickness of the water- and cast iron layers.

Global engine parameters

Table 7-1 presents parameters that are adopted from the *DCEE* concept and that are common to all simulations. Hence, these parameters are considered static inputs to the GT-Power model.

Table 7-1: Combustor properties

Engine speed [rpm]	1200
Bore [mm]	131
Stroke [mm]	158
Compression ratio	11.5
Lambda [λ]	3
Cylinder head material	Cast Iron Alloy
Mass flow through each port	58 g / s

Assumptions

- Steady state conditions are assumed.
- The exhaust ports in the simulations are completely surrounded by cooling water at a set radial distance from the ports.
- The complex geometry of the ports are simplified into individual cylinders.
- The outer boundary in each model, i.e. the last layer is always the water channel since that channel geometry is too irregular in order to make correct assessments of its layer thickness.
- Variations in outer port diameters assume that there is corresponding space to peel material from the cylinder head and potentially even the bolt pillars and the cooling water channel. This peeling will be restricted to minimum allowed thicknesses.
- The measurements of the ports are taken directly from the MD13 engine. However, in GT-Power, the ports are individually modelled in the sense that they do not merge approximately half way like in the MD13 engine, seen in figure 7. Instead, they are decoupled from each other in the model, according to figure 22.
- The water channel is set to be the last layer since the radial distance and thicknesses are somewhat regular up until that point. The cast iron layer outside of the water channel is too irregular in both distance and thickness, making it too difficult to assess in the simplified cylinder-shaped model in GT-Power.

7.1 Conventional exhaust ports

In order to maximize simulation relevance, it is important to use as correct input values as possible. Such values, describing the conventional exhaust ports geometries and inputs, can be found below in table 7-2 and 7-3, respectively. The inputs are taken from measurements of the cylinder head of the MD13 engine, which is to be used in subsequent experimental assessments. The goal of performing simulations for the conventional exhaust ports is to create reference values that can be used for comparison with the insulated setup.

The port diameter was measured at different points throughout the exhaust ports and then divided by the number of measurements in order to create a mean diameter. The same approach was utilized for the cast iron- and water thicknesses. The length of each port was measured following the center line in the CAD-model. The modelled ports, as they are interpreted in GT-Power, can be visualized in figure 22.

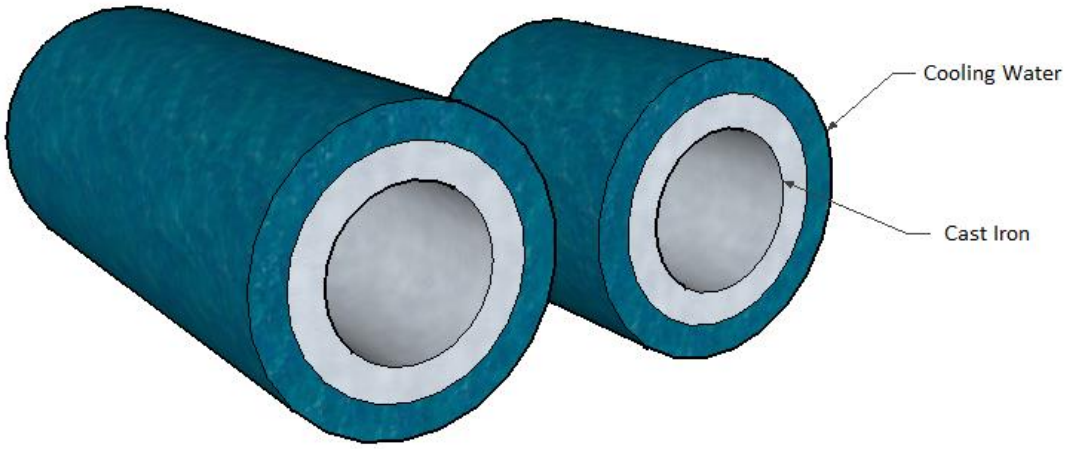

Figure 22 - Conventional exhaust ports in GT-Power

Table 7-2: Geometry of the conventional ports

Port geometry	Mean Port diameter	(43 + 41 + 43 + 32 (near valves)) / 4 ≈ 40 mm
	Exhaust valve upper diameter[3]	33 mm
	Inner port length	210 mm
	Outer port length	140 mm

[3] Required input to GT-Power that quantifies the valve plate diameter on the upper side, facing the exhaust channel.

Table 7-3: Inputs for the conventional exhaust ports [4]

Cast iron	Surface roughness	$\varepsilon_{roughness}$ = 0.26
	Average layer thickness	6 mm[5]
	Thermal conductivity	$\lambda_{cast\ iron} = 46\ \frac{W}{m*K}$ [31]
	Specific heat capacity	$c_{\ cast\ iron} = 450\ \frac{J}{kg*K}$ [31]
	Density	$\rho_{cast\ iron} = 7200\ \frac{kg}{m^3}$ [31]
Water channel	Emittance factor	$\varepsilon_{emittance,water}$ = 0.95 [35]
	Average layer thickness	(4.29 + 21.07 + 11.23 + 7.34) / 4 ≈ 11 mm
	Cooling temperature	95 °C
	External convection coefficient	$\alpha_{water} = 6000\ \frac{W}{m^2*K}$ [24]

7.1.1.1 Results in GT-Power

The simulations are done in sweeps with varying exhaust port diameters. As stated in table 7-2, the mean port diameter of the MD13 engine is 40 mm, with an average cast iron layer thickness of 6 mm. In the following simulations, these two measurements are varied in order to study the heat transfer's dependency on the port diameters. The geometrical constraint for the sweeps is induced by the geometry of the water channel and the thinnest allowable thickness of the cast iron layer, separating the exhaust gases and the cooling fluid, set to 3 mm [25]. With these prerequisites, the total diameter of the ports including the cast iron layer is fixed to 52 mm ($40 + 6 * 2$), which is equal to the current geometry of the MD13 cylinder head. Hence, the following simulations are conducted:

Table 7-4: Simulated sweeps, with case 4 being the current geometry of the MD13 exhaust ports

Case	**1**	**2**	**3**	**4**	**5**	**6**	**7**
Port Diameter [mm]	34	36	38	40	42	44	46
Cast iron thickness [mm]	9	8	7	6	5	4	3
Total diameter [mm]	52	52	52	52	52	52	52

Figure 23 and 24 show how much the bulk temperature of the exhaust gases decrease through each individual port. The inlet gas temperature for a given diameter is more or less the same in both ports, potentially differing due to different pressure traces up- and downstream since the ports have different lengths. However, it can be seen that the outlet temperature is significantly higher in the outer port.

[4] The thickness, length and diameters were evaluated using the CAD-model of the cylinder head.
[5] The thinnest cast iron thickness found was 5.923 mm, making this a geometrical restraint when increasing port diameters.

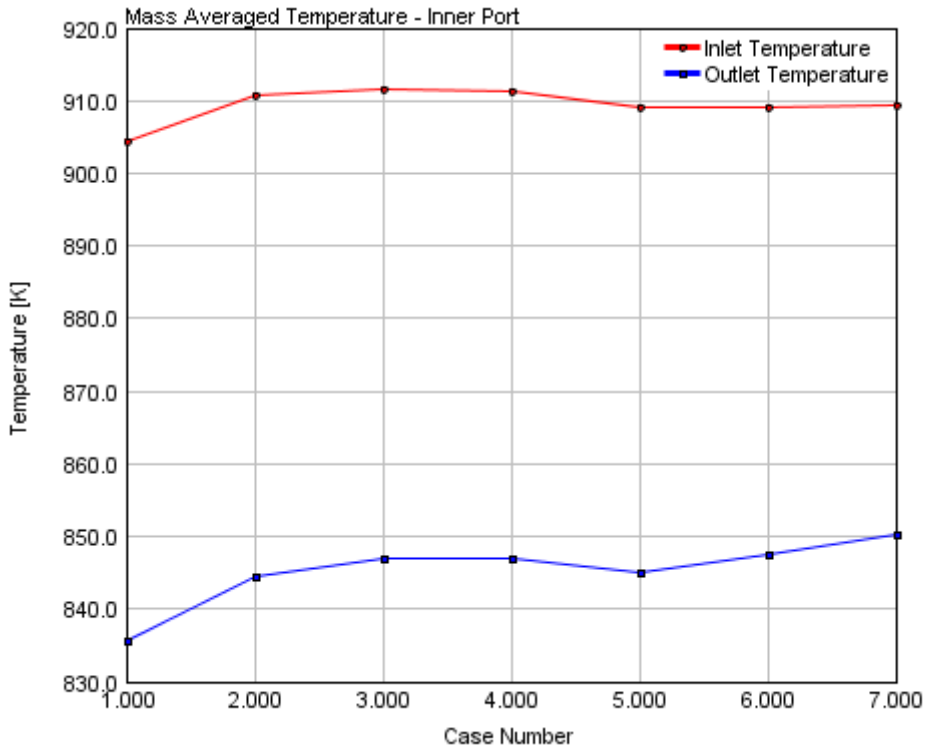

Figure 23 - Mass averaged temperature difference between the inlet and outlet of the inner port

For a fixed diameter (fixed case), the inner port intuitively experiences a greater loss in temperature compared to the shorter outer port since length scales linearly with available wall area. Hence, more surface is available for heat flux in the inner port, allowing greater radial dissipation of heat.

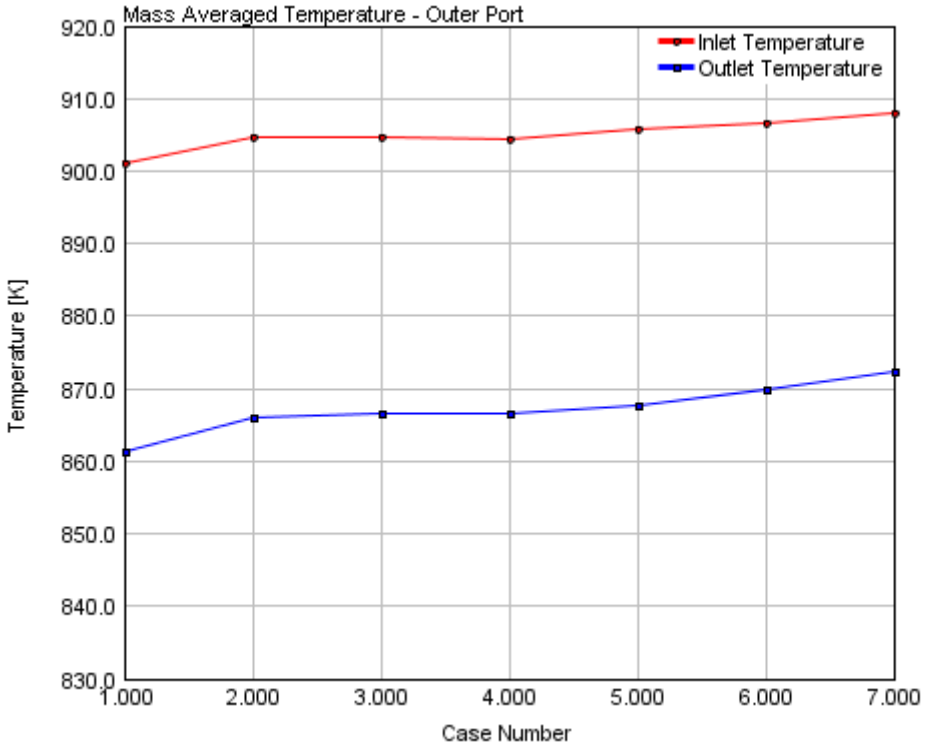

Figure 24 - Mass averaged temperature difference between the inlet and outlet of the outer port

The total temperature drop in each port is summarized for each case in table 7-5. It can be seen that both ports experience a slight tendency of less temperature drop with increasing flow diameter. As a result, the merging temperature also increases with increasing flow diameter. This phenomena is most likely related to the decrease in flow velocity as the diameter increases while having a fixed mass flow. This decreases the friction factor and the convective heat transfer according to Reynold's analogy. This effect is only partially cancelled by the fact that the surface area available for heat flux increases with increasing diameter, i.e. the decrease in flow velocity is more significant than the increase in surface area. In addition, increase of flow diameter is also more significant than the decreasing thickness of the cast iron layer, generating a more aggressive temperature gradient between the exhaust gases and the cooling water.

Table 7-5: Total Temperature drops across the exhaust ports

Case	**1**	**2**	**3**	**4**	**5**	**6**	**7**
Inner Port Temperature Drop [K]	68.647	66.259	64.661	64.457	64.071	61.669	59.024
Outer Port Temperature Drop [K]	39.971	38.483	38.041	37.874	38.024	36.737	35.747
Merging Temperature [K][6]	840	847	849	849	849	852	855

In analogy with the temperature drop, there is also a pressure drop in each channel. This pressure drop is depicted for both ports in figure 25. As can be seen, the pressure drop is higher across the shorter outer channel, at least for lower port diameters. At case 5 (42 mm in flow diameter) the pressure drop is suddenly higher in the longer inner port. True for both ports is that the pressure drop decreases with increasing port diameter, but with decreasing slope. This type of decreasing pressure drop correlates intuitively with the decreasing temperature drops. However, the switch at case 5 is harder to interpret, but the difference in pressure drop between each port is not significant. The switch could just be related to numerical deviations in the model.

[6] The ports eventually merge in the GT-Power model, resulting in a common temperature and pressure

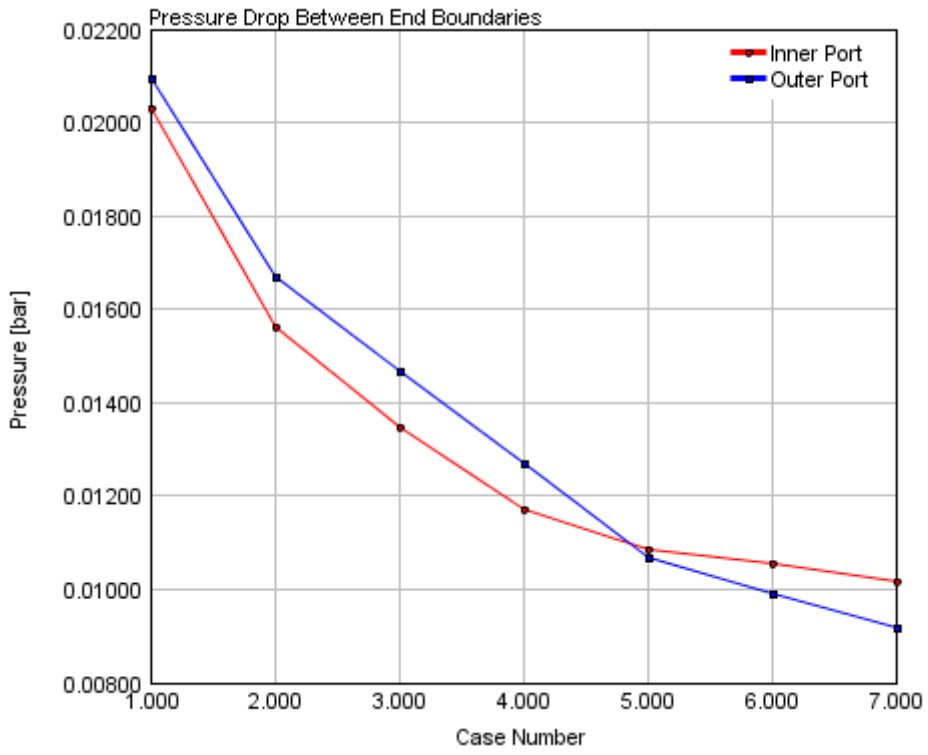

Figure 25 - Pressure Drop between end boundaries in each port

The pressure drop is realized in absolute values in table 7-6, including the final merging pressure further downstream from the exhaust ports. In analogy with the temperature, the pressure drop decreases and the merging pressure is higher with larger flow diameters.

Table 7-6: Pressure drop across each port

Case	1	2	3	4	5	6	7
Inner Port Pressure Drop [bar]	0.0203	0.0156	0.0135	0.0117	0.0109	0.0106	0.0102
Outer Port Pressure Drop [bar]	0.0209	0.0167	0.0147	0.0128	0.0107	0.0099	0.0092
Merging Pressure [bar][4]	13.9632	14.0628	14.0903	14.0798	14.0697	14.1101	14.1313

Figure 26 shows the heat transfer dynamics in each port as a function of the engine's crank angle. The dynamics can be split into two parts, one that is calmer and one that oscillates with high peak values. The calmer sections before 180- and after 360 degrees are characterized by lower heat transfer since the valves are shut, leaving remnant gases trapped and at rest within the ports. Just after 180 degrees, the valves open during the exhaust stroke, allowing newly burnt gases from the cylinder to flow into and past the ports, generating high convective heat transfer. This is represented by the spikes in figure 26, reaching peaks of around 23- and 21 kW in the outer- and inner port, respectively. However, it is to be kept in mind that this heat transfer is calculated per sub volume, i.e. it says nothing about the total heat transfer in each port. Another thing to note is that the peaks generated by each case are hard to distinguish from each other, indicating a narrow window of change in the dynamic heat transfer for the different cases.

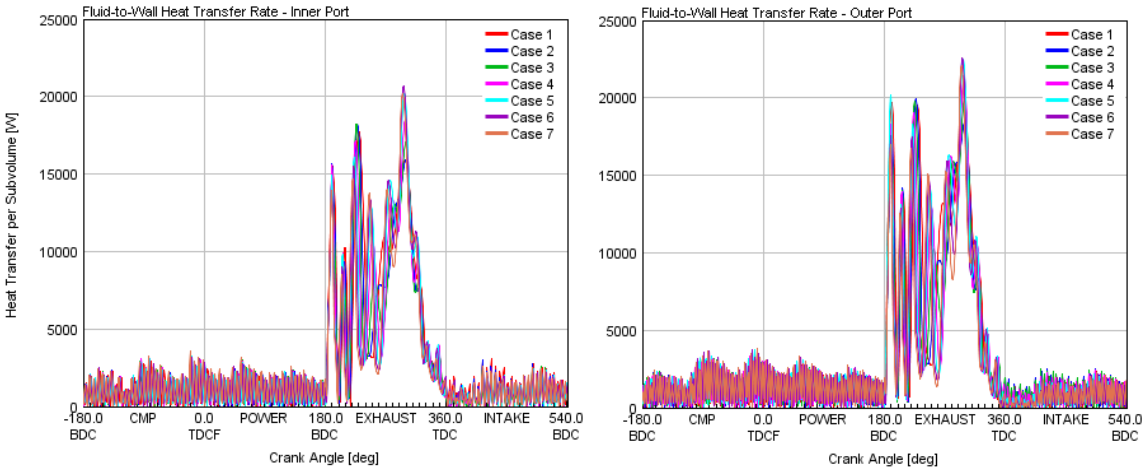

Figure 26 - Fluid-to-Wall Heat Transfer Rate in each port as a function of Crank Angle

As can be seen in figure 27, the average wall temperature decreases as the flow area is increased and the cast iron thickness is decreased. Interesting to note is also that the outer port wall temperatures are higher than in the inner port. This temperature gap narrows with increasing case number and in case 6 and 7, each port has almost identical wall temperatures. Although the increments in diameter and cast iron thickness in both ports are the same with increasing case number, each port will have different ratios of length divided by diameter. Naturally, the ports will be affected differently with each increment.

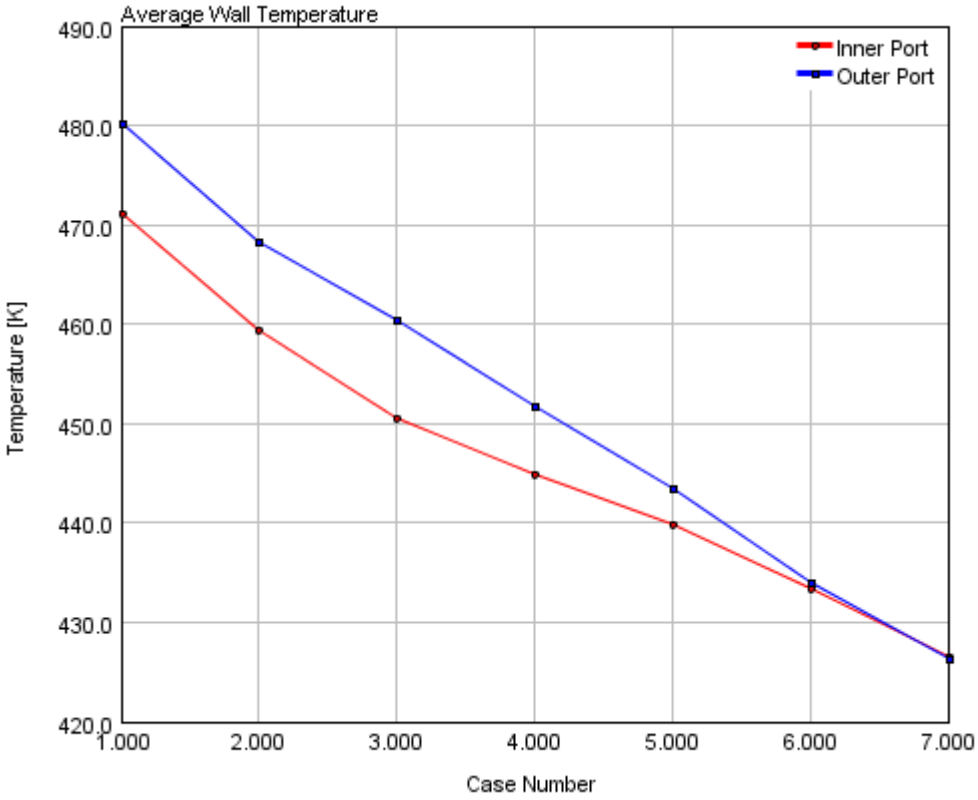

Figure 27 - Average Wall Temperature in each port as a function of the different cases

The decreasing heat flux in each port, visible in figure 28, correlates well with the decreasing wall temperature in figure 27. This is further validated by the fact that the mutual order between the two ports is the same in each figure.

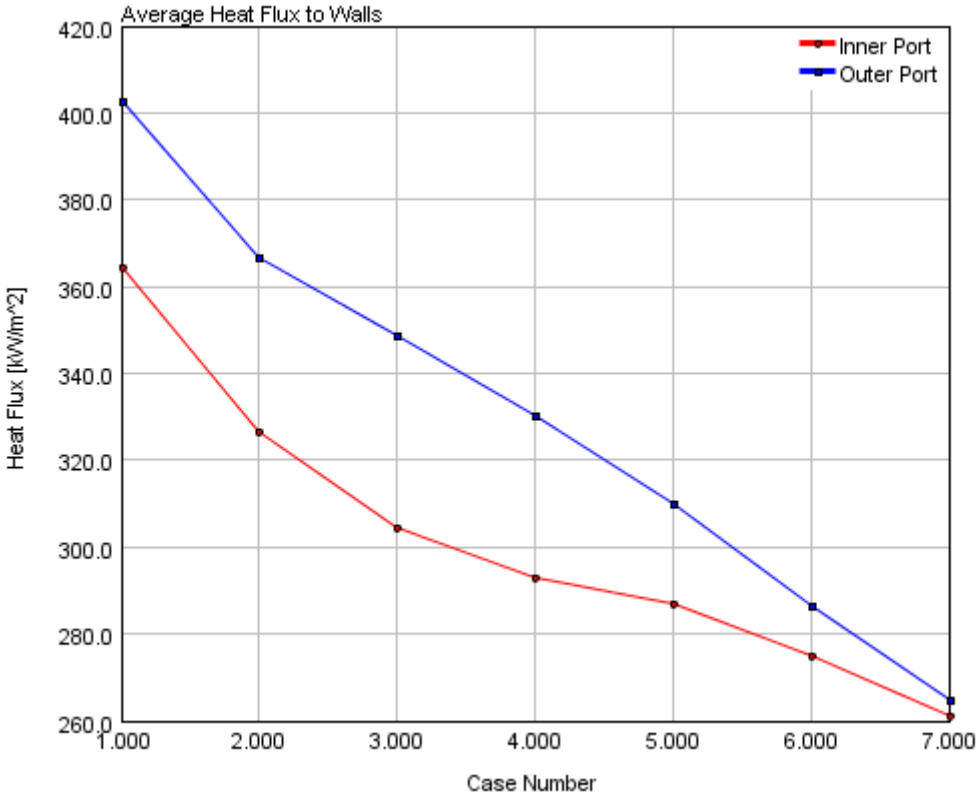

Figure 28 - Average heat Flux to Walls in each port as a function of the different cases

The total heat rate leaving the exhaust gases is visualized in figure 29, accounting for all heat transfer mechanisms; convection, conduction and radiation. Note that the figure accounts for the entire mantle area in each port and that the values are based on average heat transfer.

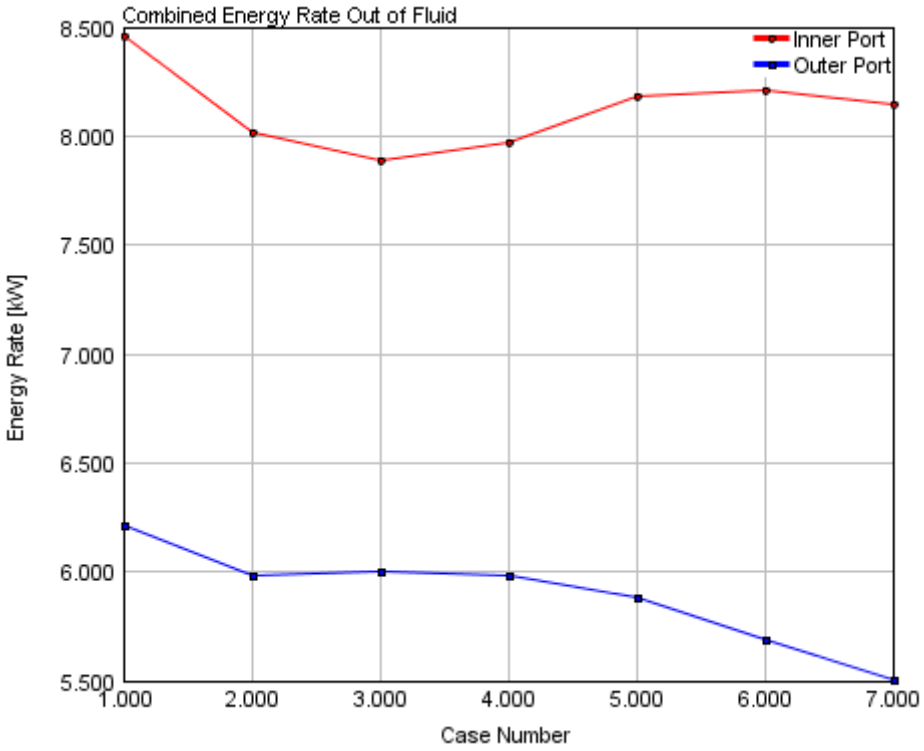

Figure 29 – Combined energy rate out of the exhaust gases in each port[7]

Figure 29 depicts a rather peculiar outcome, where the inner and outer port seem to behave differently with the different cases with regard to the radial energy rate out of the exhausts. With increasing port diameter, the heat losses initially decrease, which is intuitive if one consider that the flow is less obstructed by a low cross-area as the diameter increase. As discussed, this phenomena is covered in the Moody Diagram and is linked to a lower friction factor that ultimately reduces the convective heat losses. In fact, the convective heat flux reduces steadily from case 1 to 7, as shown in figure 28. However, the decreasing energy rate is more continuous in the outer port, while the opposite occurs in the inner port after case 3. In the inner port, this can be explained by the fact that the increasing diameter results in a more significant increase in mantle area compared to the decreasing heat flux. As a result, the net heat loss starts to increase instead. In the outer port, the increase in flow diameter is more significant than the increase of mantle area. Once again, the different behavior in each port is inherited from different lengths.

The individual heat transfer rates between the exhaust gas and the cooling fluid, depicted in figure 29, are given in table 7-7 as a function of the simulated cases. The total heat transfer rate summarizes the heat losses in both port and will be used for comparison in subsequent chapters. As can be seen in table 7-7, case 3 with a flowing diameter of 38 mm generated the lowest overall heat transfer losses.

[7] The combined energy rate out of the fluid (exhausts) also account for around 250 W heat loss, in each case, to the exhaust valves. It does not account for any radiative heat loss directly to the inner walls, but is affected through the steady state condition by radiative and convective heat losses to the ambient cooling water.

Table 7-7: Combined energy rate leaving the exhaust ports

Case	1	2	3	4	5	6	7
Inner Port (kW)	8.46133	8.01773	7.89017	7.96891	8.18223	8.21083	9.14943
Outer Port (kW)	6.21373	5.98667	6.00504	5.98039	5.88224	5.69169	5.50203
Total Heat Transfer Rate in both Ports (kW)	14.67506	14.00440	13.89521	13.94930	14.06447	13.90252	14.65146

7.2 Insulated exhaust ports

For the insulated exhaust ports, it was necessary to complement with additional data that relates to the additional metallic layer as well as the insulating ceramic material, according to the chosen insulation concept in chapter 6.3. The total input data used, as well as a visualization of the ports are given in table 7-9 and figure 30, respectively.

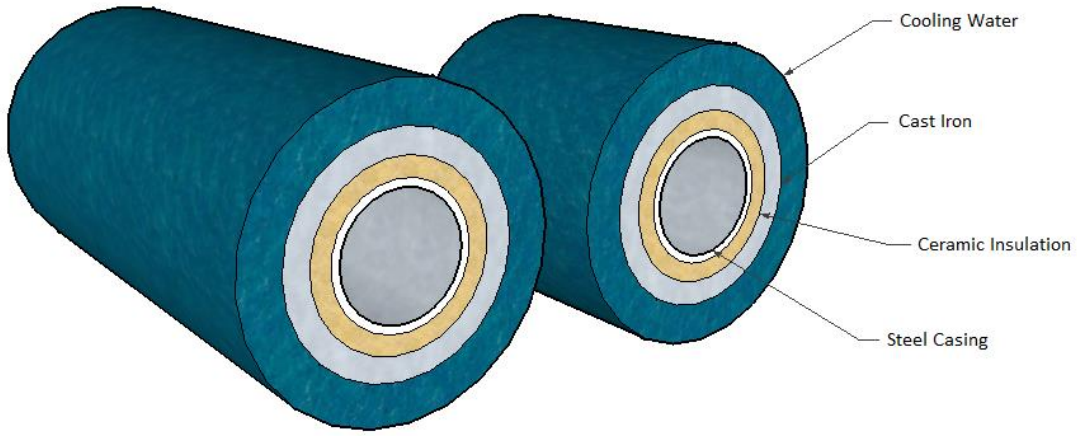

Figure 30 - Insulated exhaust ports in GT-Power

From the conventional simulations, it was concluded that the average flow diameter of 38 mm resulted in the lowest heat transfer losses from the exhaust gas. Still, the mean measured diameter of the MD13 ports was estimated to 40 mm. However, this should not be treated as absolute fact since it's only a weighted value of a few points. Hence, using 38 mm as basis for these simulations instead of 40 mm is considered within the range of standard deviation from the manual measurements. With this in mind, along with the fact that 38 mm produced the best results, the cases for these simulation sweeps will be based on a flowing diameter of 38 mm. In addition, there is no geometrical restriction in reducing the diameter inwards, only outwards due to potential entry to the water channel and scraping of cylinder bolts.

The sweep cases can be visualized in table 7-8 below. The steel plate thickness is kept at 1.5 mm for practical purposes linked to manufacturing [36]. That leaves two variables available for sweeping, i.e. insulation- and cast iron thickness.

Table 7-8: Different simulated case setups

Case	**1**	**2**	**3**	**4**	**5**	**6**	**7**
Port Diameter [mm]	38	38	38	38	38	38	38
Steel plate thickness [mm]	1.5	1.5	1.5	1.5	1.5	1.5	1.5
Ceramic Insulation [mm]	1	1.5	2	2.5	3	3.5	4
Cast iron thickness [mm]	4.5	4	3.5	3	2.5	2	1.5
Total diameter [mm]	52	52	52	52	52	52	52

Table 7-9: Inputs for the insulated exhaust ports

Steel plate	Surface roughness	$\varepsilon_{roughness} = 0.046$
	Layer thickness	$t = 1.5\ mm$
	Thermal conductivity	$\lambda_{stainless\ steel} = 15\ \frac{W}{m*K}$ [37]
	Specific heat capacity	$c_{stainless\ steel} = 500\ \frac{J}{kg*K}$ [37]
	Density	$\rho_{stainless\ steel} = 7640\ \frac{kg}{m^3}$ [37]
	Emittance factor	0.54 [35]
Ceramic insulation	Surface roughness	[-]
	Layer thickness	$[1{,}1.5, \ldots.,4]\ mm$
	Thermal conductivity	$\lambda_{ceramic\ insulation} = 0.2\ \frac{W}{m*K}$ [38]
	Specific heat capacity	$c_{ceramic\ insulation} = 1046.7\ \frac{J}{kg*K}$ [38]
	Density	$\rho_{ceramic\ insulation} = 3000\ \frac{kg}{m^3}$ [38]
	Emittance factor	0.35 [39]
Cast iron	Surface roughness	[-]
	Layer thickness	$[4.5, 4.0, \ldots, 1.5]\ mm$
	Thermal conductivity	$\lambda_{cast\ iron} = 46\ \frac{W}{m*K}$ [31]
	Specific heat capacity	$c_{\ cast\ iron} = 450\ \frac{J}{kg*K}$ [31]
	Density	$\rho_{cast\ iron} = 7200\ \frac{kg}{m^3}$ [31]
	Emittance factor	0.81 [40]
Water channel[8]	Surface roughness	[-]
	Average layer thickness	(4,29 + 21 + 11,23 + 7) / 4 = 11 mm
	Thermal conductivity	[-]
	Specific heat capacity	[-]
	Density	[-]
	Emittance factor	0.95 [35]
	Cooling temperature	95 °C
	External convection coefficient (α_{water})	$\alpha_{water} = 6000\ \frac{W}{m^2*K}$ [24]

[8] Since the water channel constitutes the last layer, dissipated heat will not travel through it, resulting in less required input.

7.2.1.1 Results in GT-Power

The mass averaged temperature drop in each port is visualized in figure 31 and 32. Compared to the conventional setup, the temperature drop is significantly lower for all cases. The same slight tendency of reduced temperature drop with increasing case remains. However, the cases are now functions of the relative thickness ratio between the insulation- and the cast iron thickness. The flow diameter is fixed at 38 mm for all cases.

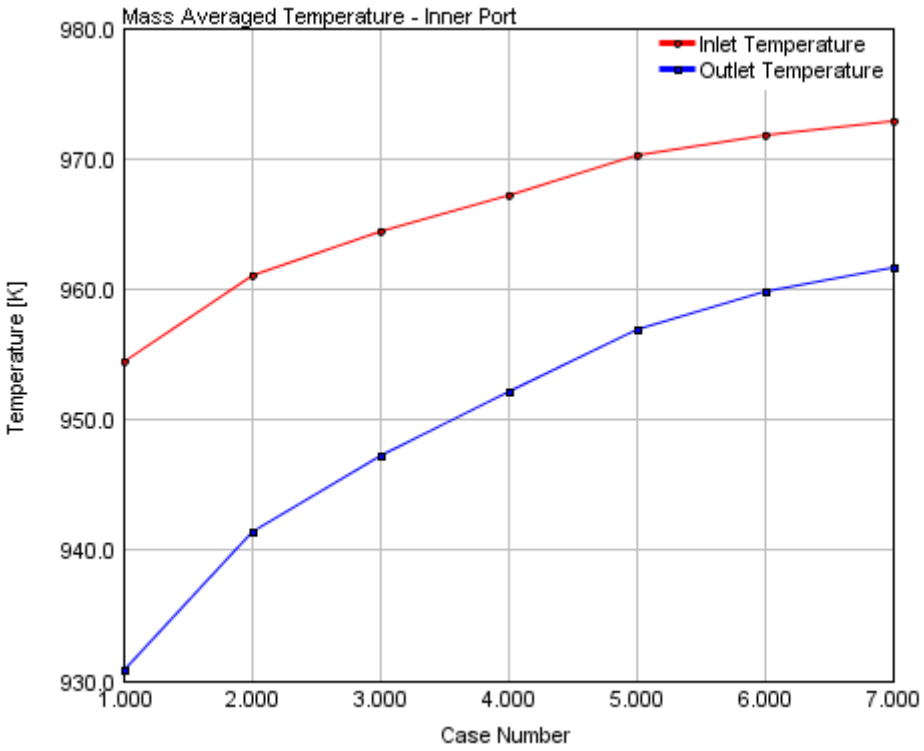

Figure 31 - Mass Averaged Temperature between end boundaries in the inner port

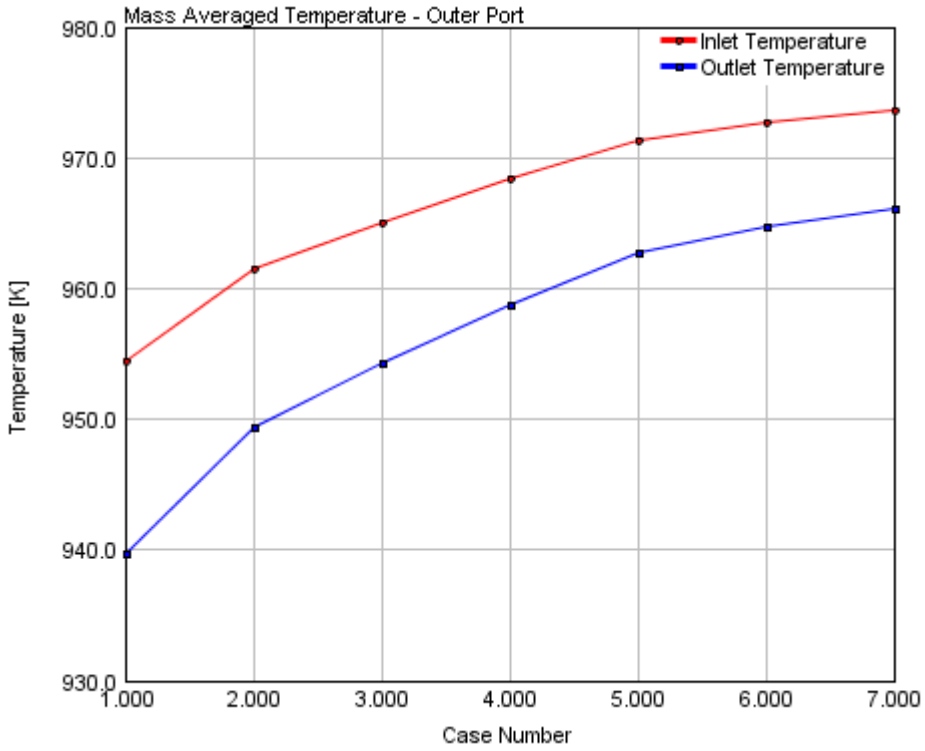

Figure 32 - Mass Averaged Temperature between end boundaries in the outer port

Apart from the actual temperature drop across the ports, the inlet temperatures are also higher in comparison to the conventional ports even though the only difference lies in the design of the ports themselves. This is related to the fact that newly burnt gases from the cylinder are being discharged into a generally hotter environment as a result of insulation. Numerically, this generates a new temperature equilibrium and hence a new and higher inlet temperature.

The temperature drop as a function of the insulation to cast iron ratio can be visualized in absolute numbers in table 7-10. Intuitively, the positive increments of insulation thickness has larger significance to the heat losses than the corresponding decrease in cast iron thickness, as the temperature drop decreases and the merging temperature increases with case number.

Table 7-10: Temperature Drop between end boundaries in each port

Case	**1**	**2**	**3**	**4**	**5**	**6**	**7**
Inner Port Temperature Drop [K]	23.699	19.647	17.137	15.061	13.226	12.060	11.231
Outer Port Temperature Drop [K]	14.758	12.166	10.815	9.664	8.611	7.984	7.512
Merging Temperature [K]	920	929	934	939	944	947	949

The pressure drop for the insulated ports is depicted in figure 33, intuitively following the same pattern as the temperature drop. It is possible to see that the steep gradient between case 1 and 2 in figure 33 correlates well with the largest increase in merging temperature between corresponding cases in table 7-10. Similar phenomena can be seen between case 6 and 7, where a flat gradient corresponds to a small increase in merging temperature.

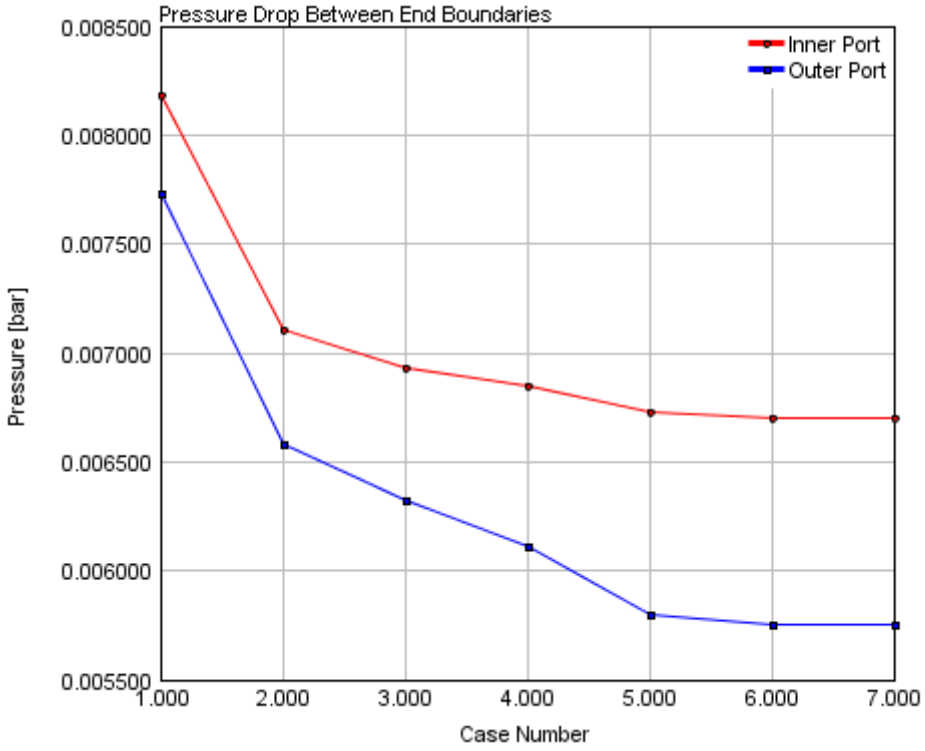

Figure 33 - Pressure Drop between end boundaries in each port

The pressure drop is realized in absolute values in table 7-11, including the final merging pressure further downstream from the exhaust ports. In analogy with the temperature, the pressure drop decreases, generating higher merging pressures with increasing insulation- to cast iron thickness ratios.

Table 7-11: Pressure Drop between end boundaries

Case	**1**	**2**	**3**	**4**	**5**	**6**	**7**
Inner Port Pressure Drop [bar]	0.00819	0.00711	0.00693	0.00684	0.00673	0.00670	0.00670
Outer Port Pressure Drop [bar]	0.00773	0.00658	0.00632	0.00611	0.00580	0.00576	0.00575
Merging Pressure [bar]	14.4011	14.5636	14.6579	14.7842	14.9160	14.9746	15.0023

Figure 34 depicts the fluid to wall heat transfer in the exhaust ports as a function of the engine's crank angle. Unlike in the conventional setup, the peak transfer rate during discharge now decreases significantly as a function of increasing case number, i.e. increasing ratio between insulation- and cast iron thickness. In addition, the heat transfer before and after discharge, when the valves are closed, is also significantly lower due to better temperature containment from the insulation.

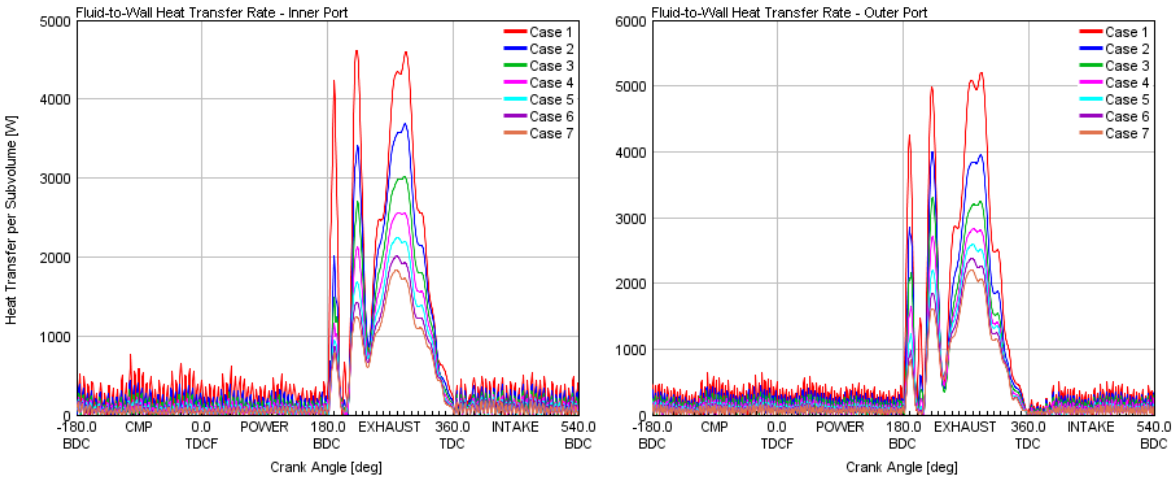

Figure 34 - Fluid-to-Wall Heat Transfer Rate in each port as a function of Crank Angle

Intuitively, the wall temperatures in each port increase with increasing insulation thickness, according to figure 35. However, the gradient of the increase flattens with each case, rendering the relative increase weaker each time the thickness increases, using the same increment each time. Once again, the increase in insulation thickness is more significant than same amount of decrease in cast iron thickness.

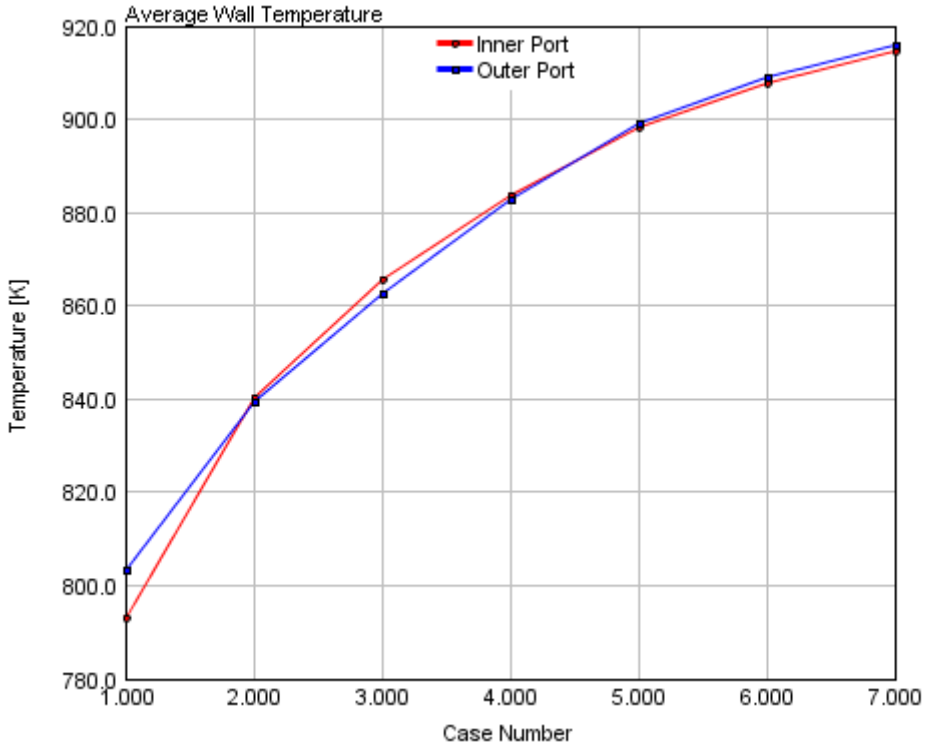

Figure 35 - Average Wall Temperature in each port as a function of the different cases

The average heat flux to the walls, visualized in figure 36, is substantially lower than in the conventional setup. Even with 1 mm insulation thickness (case 1), the heat flux is more than 3.5 times lower than the corresponding case (flow diameter of 38 mm) from the conventional and non-insulated setup. However, it must be kept in mind that a great portion of the low heat flux is credited to the effort of

every layer of the insulation, actively affecting temperature gradients that drive the convective mechanism between the gas and the inner wall.

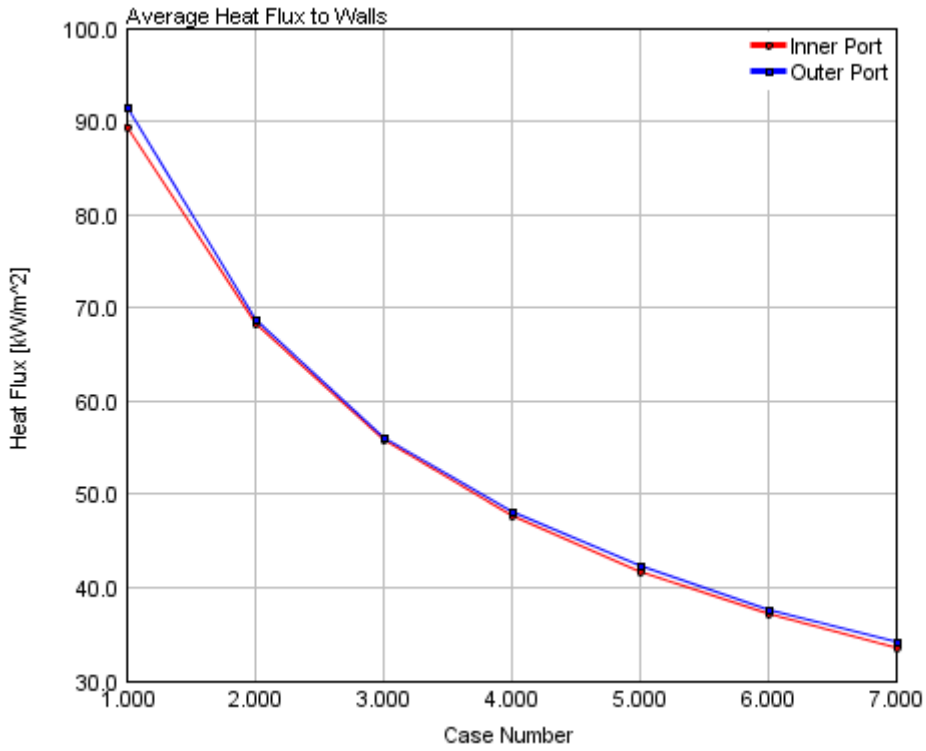

Figure 36 - Average heat Flux to Walls in each port as a function of the different cases

All in all, the total combined energy leaving the exhaust gas can be visualized in figure 37. Evidently, the energy loss is much lower than in the conventional setup, decreasing with increasing case number. This behavior is consistent in both ports, differing in magnitude only due to different port lengths and hence wall area available for heat transfer. However, the relative benefit decreases with increasing insulation- to cast iron thickness (case number), eventually reaching stagnation of potential benefit. With the given geometrical constraints to allowable thicknesses, this ultimate stagnation is not reached for the simulated cases.

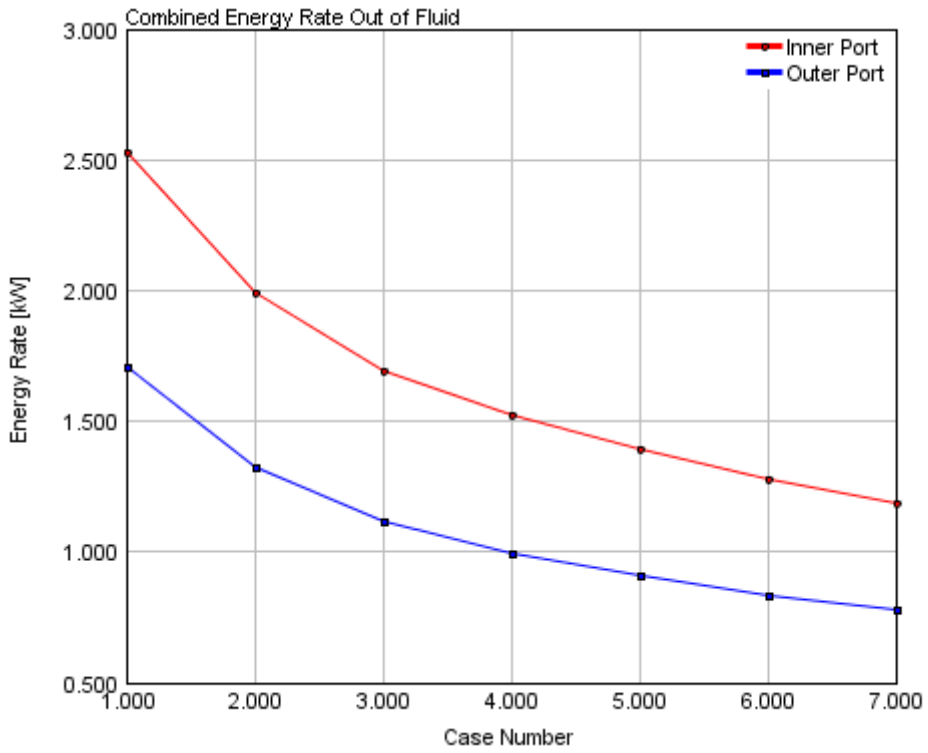

Figure 37 - Combined energy rate out of the exhaust gases in each port

The combined energy rate leaving the exhaust gas is visualized in absolute values in table 7-12. The total heat transfer rate in both ports is calculated as the sum of the individual results in each port.

Table 7-12: Combined energy rate leaving the exhaust ports

Case	1	2	3	4	5	6	7
Inner Port (kW)	2.53031	1.99118	1.69437	1.52128	1.38973	1.27982	1.18995
Outer Port (kW)	1.70817	1.32394	1.11521	0.993904	0.907183	0.834386	0.776458
Total Heat Transfer Rate in both Ports (kW)	4.23848	3.31512	2.80958	2.515184	2.296913	2.114206	1.966408

8 Validity of the simulations

The simulations are run until steady state conditions occur, meaning that the heat loss mechanisms will correlate and balance each other through the sum of all layer. Hence, an increase of the gas-to-wall convective heat loss must be balanced by the sum of increases in heat conduction through the walls and radiative heat losses. This type of steady state balance was examined and verified in every simulated case. The only thing that didn't add up was the difference in net energy through the layers and the energy leaving the gas, where a surplus number remained accounting for between 0.2-0.3 kW in each case. Upon further review, this energy remnant was accredited to the heat transfer between the gas and the exhaust valves connected to the ports, validating the total energy flow balance.

The ports are simulated as if the water channel completely covers every node along the ports. However, the circular coverage of the water channel is around 70 % according to the CAD-model. In total, the channel is missing a 30 % water coverage from a view facing the flow, as well as in the perpendicular perspective, parallel to the flow (compare figures 7 and 8). Taking both coverages into account will result in a net $0.7 \cdot 0.7 = 0.49$ ratio of overall water channel coverage. However, due to restraints in layer implementations in GT-Power, such custom coverage was not possible. This implementation would potentially alter the results in such a way that the average temperatures would have been higher in absolute values, i.e. that the heat losses would have been slightly lower than in the simulated results. However, these outcomes are also reliant on the water channel thickness, which varies significantly along the ports. All in all, the irregular geometry of the water channel was the main motivation for putting it as the last layer, requiring only boundary conditions such as temperature and external convection coefficient.

Even with a complex implementation of the channel, it would have been difficult to pinpoint potential improvements or flaws to their respective origin. With simple cylinders, conclusions are much easier to make. In addition, potential design flaws in the current model are common to both the conventional- and the insulated setup. From this perspective, results utilizing relations are arguably more valid than a single and ambiguous result, lacking data for benchmarking.

The potential need for laser puncturing is not implemented in the model, nor is it accounted for in any other way. As mentioned, this action opens up escape routes for local gas pockets generated during casting. In a practical application, this would generate additional heat losses.

8.1 Sensitivity analysis

The thermal conductivity of the saffil alumina blanket is relatively low at $0.2\ \frac{W}{mK}$. Compared to the corresponding coefficient of e.g. Zirconia, this is approximately ten times lower. Hence, it might be of interest to conduct a sensitivity analysis, using different coefficient values in order to assess the relative impact of conduction coefficient on the total energy loss through the ports. The resulting sweep of such analysis, concentrated to the ceramic insulation layer, is visualized in figure 38. The sweep is locked to case 1, starting from the results that were generated from using saffil alumina as insulation.

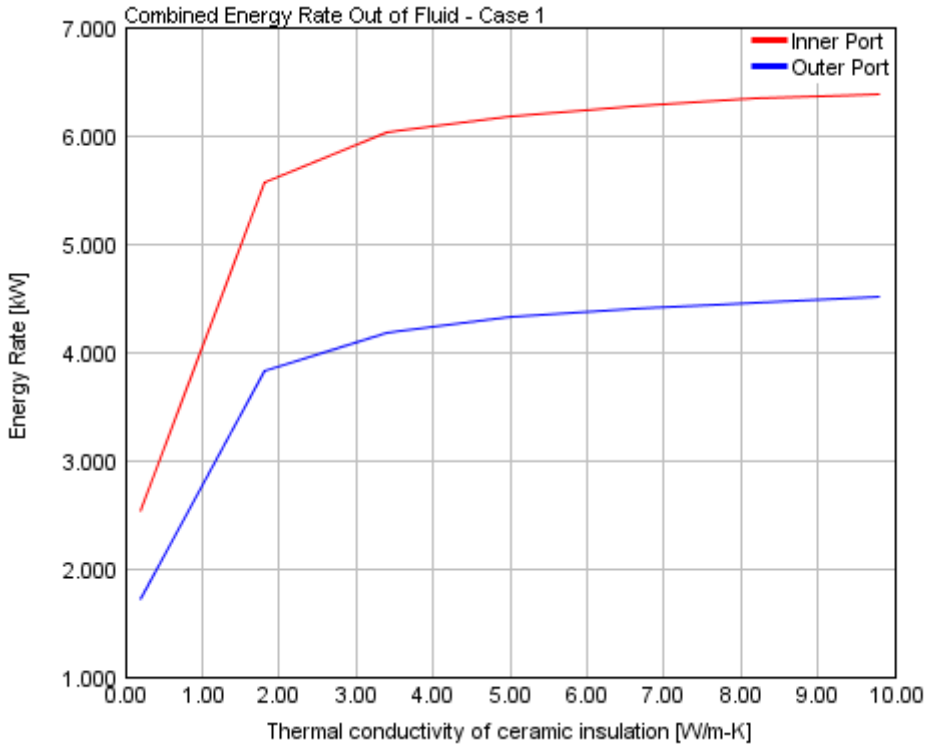

Figure 38 – Sensitivity analysis of the combined energy rate out of the exhaust gases in each port as a function of the conductivity of the ceramic insulation

From this visualization, it is clear that the conduction coefficient has high relevance to the final results. For example, using Zirconia instead of saffil alumina would more than double the energy rate leaving the fluid.

9 Comparison and conclusions

A final breakdown of the resulting heat losses in the conventional- and insulated ports can be visualized in the table below. The final row of the table states the relative decrease in overall heat losses for each case of simulations. This relative percentage is benchmarked against the conventional case that was based on the same diameter that was used in all insulated simulations, i.e. 38 mm. This flow diameter was shown to provide the lowest overall heat loss in a conventional setup, accounting for both ports.

Conventional exhaust ports							
Case	3						
Mean flow diameter [mm]	38						
Cast iron thickness [mm]	7						
Total diameter [mm]	52						
Total heat loss [kW]	13.9						
Insulated exhaust ports							
Case	1	2	3	4	5	6	7
Mean flow diameter [mm]	38	38	38	38	38	38	38
Insulation- / cast iron thickness [mm]	1 / 4.5	1.5 / 4	2 / 3.5	2.5 / 3	3 /2.5	3.5 / 2	4 / 1.5
Steel plate thickness [mm]	1.5	1.5	1.5	1.5	1.5	1.5	1.5
Total diameter [mm]	52	52	52	52	52	52	52
Total heat loss [kW]	4.2	3.3	2.8	2.5	2.3	2.1	2.0
Reduction from conventional setup [%]	69.8	76.3	79.9	82.0	83.5	84.9	85.6

The results from insulation procedures show impressive reductions, especially in the final case, displaying a heat loss reduction of 85.6 %. It is important to remember that the introduced steel plate also contributes to this number, functioning as an additional insulating barrier. However, one major drawback with this case is that is relies on using cast iron with a thickness of 1.5 mm. From a production- and robustness point of view, this thickness is considered unreliable. Hence, it is probably wise not to go below 3 mm, represented by case 4. However, considering the reduced heat losses and thus the reduced motivation for current cooling power, it might be possible to decrease some of the cooling water thickness and instead allocate that thickness to insulation. This way, it is possible to have a more reliant cast iron thickness set to 3 mm, while simultaneously adding more insulation thickness. However, the peeling of water layer thickness is dependent on actually adding insulation in order to avoid overheating. Another issue is that the thickness between the cast iron and the water channel, at its thinnest point, is only 4 mm. Hence, it is only possible to peel 1 mm of the water channel, using the same argument of robustness as for cast iron.

Another solution is to utilize the opposite radial direction in the ports, using available space inside the channel. As seen from the simulation, the insulation thickness is way more significant to the total heat loss than the right choice of flow diameter. Hence, sacrificing a few mm in diameter is well worth the increased space available for insulation. Going from 38- to 34 mm in flow diameter, with a fixed thickness of 3 mm for both the cast iron and the water channel, would yield 5.5 mm available for insulation (from a new total available diameter of 57 mm). However, one must be cautious not to choke the flow through the reduction of flow diameter.

From a cooling point of view, there are potential synergy effects to be gained from the reduction of heat losses, not only in the ports, but within the entire confinement of the engine. For example, less

cooling needed would imply a potential downsizing of the entire cooling system. This could lead to less power output required by the water pump and a smaller frontal area since less heat has to be dissipated through the frontal heat exchanger. Downsizing of this aggregate would yield less air drag and hence lower fuel consumption. In addition, higher exhaust temperatures could be beneficial for after-treatment systems, reaching required temperatures faster.

Coupled directly to the *DCEE* concept, the displayed reductions in heat loss would imply more exhaust enthalpy available for work conversion in the LP-cylinder, directly following the exhaust ports. This would ultimately increase the practical limits of the cycle in terms of overall brake efficiency.

10 References

[1] "Directorate - General for Climate," European Commission, 31 03 2014. [Online]. Available: http://ec.europa.eu/clima/policies/package/index_en.htm. [Accessed 31 03 2014].

[2] B. Johansson, Förbränningsmotorer, Lund: Division of Combustion Engines, LTH, 2006.

[3] "4-stroke Engine Concept," Publishguru, [Online]. Available: http://publishguru.files.wordpress.com/2014/05/4-strokes-of-engine-1.gif. [Accessed 09 12 2014].

[4] "2-stroke Engine Concept," Wordpress, [Online]. Available: http://prharikrishnan.files.wordpress.com/2014/05/2-stroke.gif. [Accessed 09 12 2014].

[5] N. Lam, "Double Compression Expansion Engine Concepts: A Path to High Efficiency," *SAE International,* no. 2015-04-14, 2015.

[6] B. Johansson, Ö. Andersson, P. Tunestål and M. Tunér, Combustion Engines - Volume 1, Lund: Division of Combustion Engines, LTH, 2014.

[7] Y. A. Cengel and M. A. Boles, Thermodynamics - An Engineering Approach, Third Edition, New Jersey: McGraw-Hill, 1998.

[8] B. Johnson and C. Edwards, "Exploring the Pathway to High Efficiency IC Engines through Exergy Analysis of Heat Transfer Reduction," *SAE International,* no. 2013-01-0278, 2013.

[9] B. Johansson, "Lecture on HCCI," Division of Combustion Engines, LTH, 2014.

[10] I. Truedsson, B. Johansson and M. Tunér, "Development of New Test Method for Evaluation HCCI Fuel Performance," *SAE International,* no. 2014-01-2667, p. 1, 2014.

[11] J. Hyvönen, C. Wilhelmsson and B. Johansson, "The Effect of Displacement on Air-Diluted Multi-Cylinder HCCI Engine Performance," *SAE International,* no. 2006-01-0205, pp. 14-15, 2006.

[12] B. Johansson, "Lecture on PPC," Division of Combustion Engines, LTH, 2014.

[13] V. Manente, B. Johansson and P. Tunestål, "Effects of Different Type of Gasoline Fuels on Heavy Duty Partially Premixed Combustion," *SAE International,* no. 2009-01-2668, p. 15, 2009.

[14] S. Jaichandar and P. Tamilporai, "The Status of Experimental Investigations on Low Heat Rejection Engines," *SAE International,* no. 2004-01-1453, pp. 3, 15, 2004.

[15] C.-A. Hergart, A. Louki and N. Peters, "On the Potential of Low Heat Rejection DI Diesel Engines to Reduce Tail-Pipe Emissions," *SAE International,* no. 2005-01-0920, p. 4, 2005.

[16] S. Jaichandar and P. Tamilporai, "Low Heat Rejection Engines - An Overview," *SAE International,* no. 2003-01-0405, p. 13, 2003.

[17] B. Sundén, Värmeöverföring, Lund: Studentlitteratur, 2010.

[18] H. Alvarez, Energiteknik - Del 1, Lund: Studentlitteratur, 1999.

[19] D. Foster and F. Struwe, "In-Cylinder Measurement of Particulate Radiant Heat Transfer in a Direct Injection Diesel Engine," *SAE International,* no. 2003-01-0072, p. 3, 2003.

[20] D. F. Young, B. R. Munson, T. H. Okiishi and W. W. Huebsch, Introduction to Fluid Mechanics - Fifth Edition, John Wiley & Sons Inc, 2012.

[21] "Moody Diagram Chart," Wikipedia, [Online]. Available: http://upload.wikimedia.org/wikipedia/commons/8/80/Moody_diagram.jpg. [Accessed 16 01 2015].

[22] W. D. Callister Jr. and D. G. Rethwisch, Fundamentals of Materials Science and Engineering - An integrated approach, 4th edition, John Wiley & Sons, Inc., 2012.

[23] I. Taymaz, "An Experimental Study of Energy Balance In Low Heat Rejection Diesel Engines," *Energy 31,* no. 364-371, 2006.

[24] M. Andreasson, "Insulated Exhaust Ports," *Master Thesis,* 1999.

[25] O. Lyckfeldt and S. Johanna, "E-mail Correspondence," Swerea Swedish Research, 2014-03-12.

[26] "Thermal Conductivity of Some Common Materials and Gases," Engineering Toolbox, [Online]. Available: http://www.engineeringtoolbox.com/thermal-conductivity-d_429.html. [Accessed 06 04 2015].

[27] A. J. Modi, "Experimental Study of Energy Balance in Thermal Barrier Coated Diesel Engine," *SAE International,* no. 2012-01-0389, pp. 1-3, 2012.

[28] M. G. Ojeda, V. Merzlikin, O. Sidorov and S. Kalenkov, "Regulation of the Combustion Chamber Walls Temperature with Semitransparent Heat Insulating Coatings," *SAE International,* no. 2007-24-0031, pp. 3-7, 2007.

[29] L. Bing, S. Yong and Z. Meilin, "A Study on the Structural Design and Reliability of Cylinder Head for Vehicle Engines," *SAE international,* no. 1999-01-0828, pp. 3-4, 1999.

[30] "Coefficients of Linear Thermal Expansion," Engineering Toolbox, [Online]. Available: http://www.engineeringtoolbox.com/linear-expansion-coefficients-d_95.html. [Accessed 07 04 2015].

[31] "Material Properties of Grey Cast Iron," MakeItFrom, [Online]. Available: http://www.makeitfrom.com/material-properties/Grey-Cast-Iron/. [Accessed 19 03 2015].

[32] "Material Properties of Nimonic Alloys," Special Metals Corporation, 04 September 2004. [Online]. Available: http://www.specialmetals.com/documents/Nimonic%20alloy%2080A.pdf. [Accessed 04 02 2015].

[33] M. C. Megel, "E-mail correspondence," Southwest Researh Institute, San Antonio, Texas, 2015-02-09.

[34] O. Lyckfeldt and S. Johanna, "E-mail Correspondence," Swerea Research Institute, 2015-03-26.

[35] "Emissivity Coefficients of Some Common Materials," Engineering Toolbox, [Online]. Available: http://www.engineeringtoolbox.com/emissivity-coefficients-d_447.html. [Accessed 19 03 2015].

[36] J. Fjelldal, "E-mail Correspondence," INM Mekaniska AB, 2015-03-24.

[37] "Material Properties of Stainless Steel," MakeItFrom, [Online]. Available: http://www.makeitfrom.com/material-properties/AISI-201-1.4372-S20100-Stainless-Steel/. [Accessed 17 03 2015].

[38] G. C. Wey and V. J. Tennery, "Assesment of Fibrous Insulation Materials," Department of Energy, Nashville, Tennessee, 1995.

[39] B. Imre, "www.ulaval.ca," Budapest University of Technology, [Online]. Available: http://qirt.gel.ulaval.ca/archives/qirt2008/papers/06_02_08.pdf. [Accessed 02 04 2015].

[40] "Emissivity Calues of Common Materials," Fluke Coorperation, [Online]. Available: http://support.fluke.com/find-sales/Download/Asset/3038318_6251_ENG_A_W.PDF. [Accessed 02 04 2015].